

# Learning to Coordinate: Distributed Meta-Trajectory Optimization Via Differentiable ADMM-DDP

Bingheng Wang, Yichao Gao, Tianchen Sun, and Lin Zhao

**Abstract**—Distributed trajectory optimization via ADMM-DDP is a powerful approach for coordinating multi-agent systems, but it requires extensive tuning of tightly coupled hyperparameters that jointly govern local task performance and global coordination. In this paper, we propose Learning to Coordinate (L2C), a general framework that meta-learns these hyperparameters, modeled by lightweight agent-wise neural networks, to adapt across diverse tasks and agent configurations. L2C differentiates end-to-end through the ADMM-DDP pipeline in a distributed manner. It also enables efficient meta-gradient computation by reusing DDP components such as Riccati recursions and feedback gains. These gradients correspond to the optimal solutions of distributed matrix-valued LQR problems, coordinated across agents via an auxiliary ADMM framework that becomes convex under mild assumptions. Training is further accelerated by truncating iterations and meta-learning ADMM penalty parameters optimized for rapid residual reduction, with provable Lipschitz-bounded gradient errors. On a challenging cooperative aerial transport task, L2C generates dynamically feasible trajectories in high-fidelity simulation using IsaacSIM, reconfigures quadrotor formations for safe 6-DoF load manipulation in tight spaces, and adapts robustly to varying team sizes and task conditions, while achieving up to 88% faster gradient computation than state-of-the-art methods.

**Index Terms**—Trajectory optimization, multiagent systems, Meta-learning, Differential dynamic programming.

## SUPPLEMENTARY MATERIAL

The source code of this work is available at [https://github.com/BinghengNUS/Learning\\_to\\_Coordinate\\_1/tree/main](https://github.com/BinghengNUS/Learning_to_Coordinate_1/tree/main).

## I. INTRODUCTION

**T**RAJECTORY optimization is critical in robotic operation, providing reference and feedforward trajectories for downstream controllers. In multiagent coordination tasks such as aerial transport of a cable-suspended load [1], multi-arm manipulation [2], and legged locomotion [3], trajectory optimization must ensure that each agent respects its own dynamics while coordinating with others through inter-agent constraints. These include managing cable tensions, synchronizing contact forces, and maintaining formations. Effective multiagent trajectory optimization demands fast computation, scalability with the number of agents, and adaptability to varying tasks, while minimizing manual design and tuning effort.

Centralized trajectory optimization provides globally consistent solutions [4], but scales poorly with the number of agents. Distributed methods address this by decomposing the

The authors are with the Department of Electrical and Computer Engineering, National University of Singapore, Singapore 117583, Singapore (email: wangbingheng@u.nus.edu, yichao\_gao@u.nus.edu, tianc.s@nus.edu.sg, elezhli@nus.edu.sg).

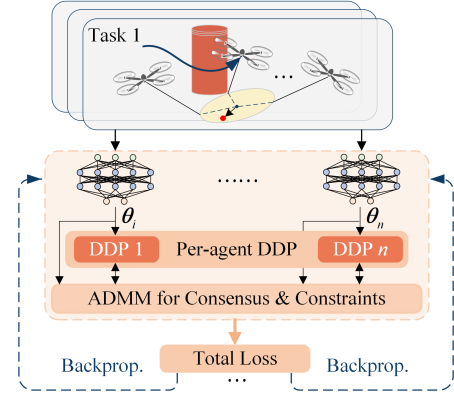


Fig. 1: The Learning to Coordinate (L2C) framework via differentiable ADMM and DDP for multiagent distributed meta-trajectory optimization. We integrate lightweight, agent-wise neural networks into the ADMM-DDP pipeline to make its key parameters adaptive to varying task objectives and numbers of agents. These networks are efficiently trained by differentiating through the entire pipeline in a distributed manner. At the core of our algorithm is an ADMM-based distributed gradient solver, enabling efficient meta-learning. Applied to a multilift system, L2C generates dynamically feasible trajectories and adapts to different team sizes and load dynamics without extra tuning.

global problem into agent-wise local subproblems linked by coordination constraints. The Alternating Direction Method of Multipliers (ADMM) handles such constraints by iteratively penalizing their violations via augmented Lagrangian terms [5]. ADMM has been widely adopted in distributed planning and control [6]–[9]. A recent work [10] combines ADMM with Differential Dynamic Programming (DDP), where DDP solves each agent’s subproblem and ADMM enforces the coordination. DDP offers robustness for trajectory optimization through convergence guarantees and feedback policies [11]–[17], the latter of which can also be used for closed-loop tracking to refine each agent’s subproblem efficiently [10].

However, jointly using DDP and ADMM requires tuning a large number of hyperparameters that grow nonlinearly with system size. These include DDP cost weights, reference waypoints, system dynamics, constraint bounds, and ADMM penalty parameters. These parameters are tightly coupled and affect both local agent behavior and global coordination. ADMM modifies each agent’s cost by penalizing deviations from consensus, directly shaping the optimization landscape of DDP. As a result, hyperparameter tuning becomes a high-dimensional, nonlinear, system-wide task. In practice, it is often performed manually [10], [18], [19], relying heavily on expert intuition, which typically results in suboptimal performance, poor scalability, and limited generalization across tasks.

The difficulty of tuning is especially pronounced in multia-

gent systems with strong couplings. A representative example is the multilift system [20]–[27], where multiple quadrotors cooperatively transport a cable-suspended load (see top of Fig. 1). The cables induce tightly coupled dynamics between the load and each quadrotor through tensions, and impose nontrivial kinematic constraints, such as limiting each quadrotor’s workspace due to fixed cable lengths. The system is highly sensitive to both trajectory parameters and coordination strategies, making it a realistic and challenging benchmark for evaluating distributed trajectory optimization methods.

For single-agent problems, a growing body of work has explored bi-level optimization frameworks that integrate optimal control with machine learning to automate hyperparameter tuning. These frameworks consist of a lower-level solver that optimizes trajectories and an upper-level learner that adjusts hyperparameters based on trajectory quality. A central challenge lies in differentiating through the lower-level solver. Two main strategies have been developed. The first unrolls the solver as a computation graph [28], [29], enabling automatic differentiation [30] but incurring significant memory and computational overhead. The second leverages the implicit function theorem to differentiate through optimality conditions, such as the Pontryagin Maximum Principle (PMP) or the Karush-Kuhn-Tucker (KKT) conditions. Vector-Jacobian product (VJP) methods compute scalar-loss gradients of the upper-level objective with respect to (w.r.t.) the solver’s hyperparameters without forming full trajectory gradients [31]–[34]. While VJP methods can be extended to multiagent systems in a centralized fashion, they fall short in distributed settings that require coordinated gradient updates across agents. Full Jacobian approaches, such as Pontryagin Differential Programming (PDP) [35], explicitly compute trajectory gradients recursively and have been extended to handle constraints [36], noise measurements [37], and DDP [38]. However, they are typically slower and more memory-intensive, as gradient computation requires solving auxiliary matrix-valued optimization problems.

In parallel, differentiable ADMM methods have been developed for static convex optimization problems [39]–[41]. One recent work applies differentiable ADMM to hyperparameter tuning in linear MPC, reformulating it as a static quadratic program with stacked trajectory variables [42]. While effective in the convex linear case, these approaches do not address robot trajectory optimization, which is characterized by nonlinear system dynamics, long-horizon coupling between states and controls, nonconvex constraints, and inter-agent coordination in multiagent systems.

In this paper, we propose Learning to Coordinate (L2C), a general framework for distributed meta-trajectory optimization that adapts across diverse tasks and scales with the number of agents (see Fig. 1). At its core, L2C differentiates through the ADMM-DDP pipeline to jointly meta-learn all hyperparameters that influence both trajectory quality and inter-agent coordination, such as DDP cost weights and ADMM penalty parameters. These hyperparameters are modeled by lightweight, agent-wise neural networks, which are trained in a distributed manner using the analytical gradients from this differentiable pipeline. L2C leverages the strengths of both model-based and model-free methods, i.e., the convergence

guarantees and explainability of first-principles distributed optimal control, and the representational flexibility of neural networks. Unlike multiagent reinforcement learning (MARL) methods [43]–[47], which estimate gradients via trial-and-error sampling and thus require large datasets, L2C enables data-efficient training, better generalization, and direct exploitation of system structure in safety-critical settings.

Compared to VJP methods, our approach retains full trajectory gradient information, enabling agent-wise meta-learning. Theoretically, it is equivalent to PDP due to the symmetry between PMP and Bellman’s principle of optimality, yet achieves significantly greater efficiency in practice. This arises from reusing key DDP components, such as Riccati recursions and feedback gains, computed during the forward pass. We further show that trajectory gradients correspond exactly to the optimal solutions of distributed matrix-valued Linear Quadratic Regulators (LQR), coordinated via an auxiliary ADMM framework using the same penalty parameters from the forward pass. This auxiliary problem is convex under mild assumptions, allowing us to leverage ADMM’s convergence guarantees for gradient computation. Prior works have proposed adaptive methods to improve convergence by adjusting ADMM penalty parameters during iterations [48]–[50]. Despite these efforts, they typically require dozens of iterations to meet residual tolerances. To speed up training, we truncate ADMM iterations and meta-learn the penalty parameters for fast residual minimization. We also prove that gradient errors from truncation are Lipschitz bounded, ensuring stable learning.

We validate L2C on a multilift system transporting a cable-suspended load through cluttered environments. Prior trajectory optimization methods in this domain, both centralized [51]–[57] and heuristic distributed [58], [59], depend on manually tuned objectives [53]–[56], [58], [59], fixed team sizes (three [51] or four [52] quadrotors), conservative formation shapes (e.g., pyramids [55], [57]) or hand-crafted configurations for passing through narrow passages [59]. These designs limit both adaptability and generalization. When the team size, task objectives, or load dynamics change, substantial redesign is often required. In contrast, our approach meta-learns neural adaptive ADMM-DDP hyperparameters that scale efficiently with team size and generalize across varying task conditions. It accommodates diverse load dynamics, such as shifts in the load’s center of mass that require different tension distributions and formation shapes. Training is highly efficient, our method achieves up to 88% faster gradient computation compared to state-of-the-art methods [35], [38] and converges within merely tens of episodes. We evaluate the trained ADMM-DDP trajectory optimizer in unseen environments using a high-fidelity software-in-the-loop (SITL) simulator developed with IsaacSIM [60]. It generates dynamically feasible trajectories, augmented by the DDP feedback policies, that are directly trackable via a feedback flight controller. The system autonomously reconfigures quadrotor formations (e.g., from fanning out to lining up) to enable safe 6 degree-of-freedom load manipulation through tight spaces. It further adapts robustly to variations in quadrotor counts and load dynamics without extra tuning.

We summarize the main contributions as follows.

- 1) We propose L2C, a general framework for distributed meta-trajectory optimization that automatically tunes adaptive ADMM-DDP hyperparameters in multiagent systems via gradient-based meta-learning. All key hyperparameters are modeled using lightweight, agent-wise neural networks and trained efficiently by differentiating through the entire ADMM-DDP pipeline in a distributed manner. This enables scalability with the number of agents and generalization across diverse tasks.
- 2) We show that DDP trajectory gradients correspond to the optimal solutions of a matrix-valued LQR. Leveraging this structure, we develop an efficient method to recursively compute gradients by reusing key results from the DDP solver, such as Riccati recursions and feedback gains. Compared to existing full Jacobian-based methods, our approach significantly accelerates gradient computation in long-horizon settings.
- 3) We introduce an auxiliary ADMM framework that coordinates the distributed matrix-valued LQR problems across agents. The framework reuses penalty parameters from the forward pass and becomes convex under mild conditions. To accelerate training, we truncate ADMM iterations and jointly meta-learn the penalty parameters for rapid residual reduction, with theoretical Lipschitz bounds on the resulting gradient errors.
- 4) We validate L2C on the multilift task in cluttered environments. Experiments in a high-fidelity SITL simulator demonstrate efficient training and robust adaptation to varying task conditions and team sizes, highlighting L2C's potential for large-scale multiagent systems with strong dynamic couplings.

In the remainder of the paper, Section II briefly reviews the ADMM-DDP pipeline for distributed trajectory optimization in multiagent systems. Section III formulates the proposed L2C framework. In Section IV, we derive the analytical gradients recursively and introduce an auxiliary ADMM framework to coordinate these gradients across agents. Section V applies L2C to multilift systems, and Section VI presents the experimental results. Finally, Section VII concludes the paper.

## II. PRELIMINARIES

### A. Centralized Multiagent Trajectory Optimization

Consider  $n$  robots collaborating on a task such as cooperative transport or manipulation. Their trajectories are found by minimizing the sum of local costs subject to dynamics, local constraints, and inter-agent constraints, yielding the centralized trajectory optimization problem:

$$\min_{\{\mathbf{x}_i, \mathbf{u}_i\}_{i=1}^n} \sum_{i=1}^n J_i(\mathbf{x}_i, \mathbf{u}_i) \quad (1a)$$

$$\text{s.t. } \mathbf{x}_{i,k+1} = \mathbf{f}_i(\mathbf{x}_{i,k}, \mathbf{u}_{i,k}), \mathbf{x}_{i,0} : \text{given}, \quad (1b)$$

$$\mathbf{g}_{i,k}(\mathbf{x}_{i,k}, \mathbf{u}_{i,k}) \leq 0, \quad (1c)$$

$$\mathbf{h}_{ij,k}(\mathbf{x}_{i,k}, \mathbf{x}_{j,k}, \mathbf{u}_{i,k}, \mathbf{u}_{j,k}) \leq 0, \quad (1d)$$

where  $\mathbf{x}_{i,k} \in \mathbb{R}^{n_i}$  and  $\mathbf{u}_{i,k} \in \mathbb{R}^{m_i}$  denote the state and control of robot  $i$  at time step  $k$ , with the corresponding trajectories

$\mathbf{x}_i = [\mathbf{x}_{i,0}, \dots, \mathbf{x}_{i,N}]$  and  $\mathbf{u}_i = [\mathbf{u}_{i,0}, \dots, \mathbf{u}_{i,N-1}]$  over the horizon length  $N$ . The local cost for each robot is given by:

$$J_i(\mathbf{x}_i, \mathbf{u}_i) = \sum_{k=0}^{N-1} \ell_{i,k}(\mathbf{x}_{i,k}, \mathbf{u}_{i,k}) + \ell_{i,N}(\mathbf{x}_{i,N}), \quad (2)$$

where  $\ell_{i,k} : \mathbb{R}^{n_i} \times \mathbb{R}^{m_i} \rightarrow \mathbb{R}$  and  $\ell_{i,N} : \mathbb{R}^{n_i} \rightarrow \mathbb{R}$  are the stage and terminal costs. In (1),  $\mathbf{f}_i$  denotes the  $i$ th robot's discrete-time dynamics, (1c) is the local state and control constraint, and (1d) is the inter-agent constraint ensuring safe coordination (e.g., collision avoidance or load sharing).

### B. Distributed ADMM-DDP Pipeline

The centralized problem (1) becomes computationally prohibitive for large-scale systems. ADMM offers a scalable alternative by decomposing computation and enforcing coordination iteratively. ADMM typically handles problems with separable objectives and affine constraints:

$$\min_{\mathbf{x}, \mathbf{z}} f(\mathbf{x}) + g(\mathbf{z}) \quad \text{s.t. } \mathbf{A}\mathbf{x} + \mathbf{B}\mathbf{z} = \mathbf{c}. \quad (3)$$

The classical ADMM solves (3) via:

$$\begin{aligned} \mathbf{x}^{a+1} &= \arg \min_{\mathbf{x}} \mathcal{L}(\mathbf{x}, \mathbf{z}^a, \boldsymbol{\lambda}^a), \\ \mathbf{z}^{a+1} &= \arg \min_{\mathbf{z}} \mathcal{L}(\mathbf{x}^{a+1}, \mathbf{z}, \boldsymbol{\lambda}^a), \\ \boldsymbol{\lambda}^{a+1} &= \boldsymbol{\lambda}^a + \rho(\mathbf{A}\mathbf{x}^{a+1} + \mathbf{B}\mathbf{z}^{a+1} - \mathbf{c}), \end{aligned} \quad (4)$$

where the superscript  $a \in \mathbb{N}_0$  denotes the ADMM iteration,  $\boldsymbol{\lambda}$  is the dual variable for the constraint, and  $\mathcal{L}$  is the augmented Lagrangian given by

$$\begin{aligned} \mathcal{L}(\mathbf{x}, \mathbf{z}, \boldsymbol{\lambda}) &= f(\mathbf{x}) + g(\mathbf{z}) + \boldsymbol{\lambda}^\top (\mathbf{A}\mathbf{x} + \mathbf{B}\mathbf{z} - \mathbf{c}) \\ &\quad + \frac{\rho}{2} \|\mathbf{A}\mathbf{x} + \mathbf{B}\mathbf{z} - \mathbf{c}\|_2^2, \end{aligned}$$

with  $\rho > 0$  as the ADMM penalty parameter. These updates enforce the constraint iteratively by penalizing violations while updating the dual variable (see [5] for details).

However, applying ADMM directly to multiagent trajectory optimization is challenging due to nonlinear, nonconvex inter-agent constraints in (1d). A recent work [10] addresses this by introducing *safe-copy variables*. These variables satisfy both local and inter-agent constraints, and enable affine consensus constraints, aligning the resulting problem with the standard ADMM form.

Adopting this strategy, we define safe-copy variables  $\tilde{\mathbf{x}}_{i,k} \in \mathbb{R}^{n_i}$  and  $\tilde{\mathbf{u}}_{i,k} \in \mathbb{R}^{m_i}$  for each agent's state and control. They must satisfy both the local (1c) and inter-agent (1d) constraints, and remain consensus with the original variables via:

$$\mathbf{x}_{i,k} = \tilde{\mathbf{x}}_{i,k}, \mathbf{u}_{i,k} = \tilde{\mathbf{u}}_{i,k}, \quad \forall i \in \{1, \dots, n\}. \quad (5)$$

The corresponding augmented Lagrangian is:

$$\begin{aligned} \mathcal{L}_d &= \sum_{i=1}^n J_i(\mathbf{x}_i, \mathbf{u}_i) + \mathcal{I}_{\mathbf{f}_i}(\mathbf{x}_i, \mathbf{u}_i) + \mathcal{I}_{\mathbf{g}_i}(\tilde{\mathbf{x}}_i) + \mathcal{I}_{\mathbf{b}_i}(\tilde{\mathbf{u}}_i) \\ &\quad + \mathcal{I}_{\mathbf{h}_{ij}}(\tilde{\mathbf{x}}_i, \tilde{\mathbf{x}}_j, \tilde{\mathbf{u}}_i, \tilde{\mathbf{u}}_j) + \boldsymbol{\lambda}_i^\top (\mathbf{x}_i - \tilde{\mathbf{x}}_i) \\ &\quad + \boldsymbol{\xi}_i^\top (\mathbf{u}_i - \tilde{\mathbf{u}}_i) + \frac{\rho_i}{2} \|\mathbf{x}_i - \tilde{\mathbf{x}}_i\|_2^2 + \frac{\rho_i}{2} \|\mathbf{u}_i - \tilde{\mathbf{u}}_i\|_2^2, \end{aligned} \quad (6)$$

where  $\mathcal{I}_c(\mathbf{x})$  denote an indicator function such that  $\mathcal{I}_c(\mathbf{x}) = 0$  if  $\mathbf{x} \in \mathcal{C}$ , otherwise  $\mathcal{I}_c(\mathbf{x}) = +\infty$ ,  $\boldsymbol{\lambda}_i \in \mathbb{R}^{n_i}$  and  $\boldsymbol{\xi}_i \in$

$\mathbb{R}^{m_i}$  are the dual variables for the state and control consensus constraints of agent  $i$ , respectively. The distributed formulation of problem (1) proceeds in the following three subproblems.

*Subproblem 1:* Each agent independently minimizes (6) w.r.t. its local state and control trajectories. This yields the following  $n$  dynamic optimization subproblems:

$$\begin{aligned} \{\mathbf{x}_i^*, \mathbf{u}_i^*\}^{a+1} &= \arg \min_{\mathbf{x}_i, \mathbf{u}_i} \sum_{k=0}^{N-1} \hat{\ell}_{i,k} + \hat{\ell}_{i,N} \\ \text{s.t. } \mathbf{x}_{i,k+1} &= \mathbf{f}_i(\mathbf{x}_{i,k}, \mathbf{u}_{i,k}), \mathbf{x}_{i,0} : \text{given}, \end{aligned} \quad (7)$$

where

$$\begin{aligned} \hat{\ell}_{i,k} &= \ell_{i,k}(\mathbf{x}_{i,k}, \mathbf{u}_{i,k}) + \frac{\rho_i}{2} \left\| \mathbf{x}_{i,k} - \tilde{\mathbf{x}}_{i,k}^a + \frac{\boldsymbol{\lambda}_{i,k}^a}{\rho_i} \right\|_2^2 \\ &\quad + \frac{\rho_i}{2} \left\| \mathbf{u}_{i,k} - \tilde{\mathbf{u}}_{i,k}^a + \frac{\boldsymbol{\xi}_{i,k}^a}{\rho_i} \right\|_2^2, \\ \hat{\ell}_{i,N} &= \ell_{i,N}(\mathbf{x}_{i,N}) + \frac{\rho_i}{2} \left\| \mathbf{x}_{i,N} - \tilde{\mathbf{x}}_{i,N}^a + \frac{\boldsymbol{\lambda}_{i,N}^a}{\rho_i} \right\|_2^2. \end{aligned} \quad (8)$$

*Subproblem 2:* The augmented Lagrangian (6) is minimized w.r.t. each agent's safe-copy variables. Although these variables are locally defined, they are coupled via the inter-agent constraints (1d), making the resulting optimization problem centralized at each time step. However, since the agent dynamics  $\mathbf{f}_i$  do not depend on the safe-copy variables, this subproblem becomes a static optimization that can be decomposed temporally into  $N+1$  independent subproblems, i.e., one per time step  $k = 0, \dots, N$ .

At  $k = 0, \dots, N-1$ , the stage-wise static optimization is formulated as:

$$\begin{aligned} \{\tilde{\mathbf{x}}_k^*, \tilde{\mathbf{u}}_k^*\}^{a+1} &= \arg \min_{\tilde{\mathbf{x}}_k, \tilde{\mathbf{u}}_k} \sum_{i=1}^n \left( \frac{\rho_i}{2} \left\| \mathbf{x}_{i,k}^{a+1} - \tilde{\mathbf{x}}_{i,k} + \frac{\boldsymbol{\lambda}_{i,k}^a}{\rho_i} \right\|_2^2 \right. \\ &\quad \left. + \frac{\rho_i}{2} \left\| \mathbf{u}_{i,k}^{a+1} - \tilde{\mathbf{u}}_{i,k} + \frac{\boldsymbol{\xi}_{i,k}^a}{\rho_i} \right\|_2^2 \right) \\ \text{s.t. } \mathbf{g}_{i,k}(\tilde{\mathbf{x}}_{i,k}, \tilde{\mathbf{u}}_{i,k}) &\leq 0, \\ \mathbf{h}_{ij,k}(\tilde{\mathbf{x}}_{i,k}, \tilde{\mathbf{x}}_{j,k}, \tilde{\mathbf{u}}_{i,k}, \tilde{\mathbf{u}}_{j,k}) &\leq 0. \end{aligned} \quad (9)$$

At  $k = N$ , the terminal static optimization is given by:

$$\begin{aligned} \tilde{\mathbf{x}}_N^{a+1} &= \arg \min_{\tilde{\mathbf{x}}_N} \sum_{i=1}^n \frac{\rho_i}{2} \left\| \mathbf{x}_{i,N}^{a+1} - \tilde{\mathbf{x}}_{i,N} + \frac{\boldsymbol{\lambda}_{i,N}^a}{\rho_i} \right\|_2^2 \\ \text{s.t. } \mathbf{g}_{i,N}(\tilde{\mathbf{x}}_{i,N}) &\leq 0, \\ \mathbf{h}_{ij,N}(\tilde{\mathbf{x}}_{i,N}, \tilde{\mathbf{x}}_{j,N}) &\leq 0. \end{aligned} \quad (10)$$

Note that these static subproblems can be further decentralized by augmenting each agent's safe-copy variables with local copies of other agents' variables. Let  $\tilde{\mathbf{x}}_{i,k}^a = [\tilde{\mathbf{x}}_{j,k}^a]_{j=1}^n$  denote the augmented safe-copy state of agent  $i$ , where  $\tilde{\mathbf{x}}_{i,k}^a$  is the self-copy and  $\tilde{\mathbf{x}}_{j,k}^a$ ,  $j \neq i$  are local copies of other agents' states, the same applies to the controls. This yields fully decentralized subproblems consistent with the merged distributed structure in [10]. We develop L2C using the above centralized formulation to minimize the numbers of safe-copy variables. But it can naturally extend to the fully decentralized case via the augmented safe-copy formulation.

*Subproblem 3:* At each time step, each agent updates its own dual variables independently according to:

$$\boldsymbol{\lambda}_{i,k}^{a+1} = \boldsymbol{\lambda}_{i,k}^a + \rho_i(\mathbf{x}_{i,k}^{a+1} - \tilde{\mathbf{x}}_{i,k}^{a+1}), \quad (11a)$$

$$\boldsymbol{\xi}_{i,k}^{a+1} = \boldsymbol{\xi}_{i,k}^a + \rho_i(\mathbf{u}_{i,k}^{a+1} - \tilde{\mathbf{u}}_{i,k}^{a+1}). \quad (11b)$$

The dynamic optimization problem (7) can be efficiently solved via DDP, a second order trajectory optimization method based on Bellman's principle [61]. It states that any remaining segment of an optimal trajectory is itself optimal, enabling decomposition into smaller subproblems. This principle leads to a recursive formulation of the value function, or optimal cost to go, representing the minimum cumulative cost from a given state. For agent  $i$ , the value function at ADMM iteration  $a$  and time step  $k$  is defined as

$$\hat{V}_{i,k}^a(\mathbf{x}_{i,k}) = \min_{\mathbf{u}_{i,k}} \hat{Q}_{i,k}^a(\mathbf{x}_{i,k}, \mathbf{u}_{i,k}), \quad (12)$$

where the Q-function (cost-to-go) is defined using the augmented stage cost (8) as

$$\begin{aligned} \hat{Q}_{i,k}^a(\mathbf{x}_{i,k}, \mathbf{u}_{i,k}) &= \hat{\ell}_{i,k}^a(\mathbf{x}_{i,k}, \mathbf{u}_{i,k}, \tilde{\mathbf{x}}_{i,k}^a, \tilde{\mathbf{u}}_{i,k}^a, \boldsymbol{\lambda}_{i,k}^a, \boldsymbol{\xi}_{i,k}^a) \\ &\quad + \hat{V}_{i,k+1}^a(\mathbf{f}_i(\mathbf{x}_{i,k}, \mathbf{u}_{i,k})), \end{aligned} \quad (13)$$

with terminal condition

$$\hat{V}_{i,N}^a(\mathbf{x}_{i,N}) = \hat{\ell}_{i,N}^a(\mathbf{x}_{i,N}, \tilde{\mathbf{x}}_{i,N}^a, \boldsymbol{\lambda}_{i,N}^a). \quad (14)$$

Instead of solving the Bellman optimality equation (12) exactly, DDP approximates the system dynamics and value function to second order around normal trajectories  $\{\bar{\mathbf{x}}_i, \bar{\mathbf{u}}_i\}$ . Defining the deviations as  $\delta \mathbf{x}_{i,k} = \mathbf{x}_{i,k} - \bar{\mathbf{x}}_{i,k}$  and  $\delta \mathbf{u}_{i,k} = \mathbf{u}_{i,k} - \bar{\mathbf{u}}_{i,k}$ , we obtain the quadratic approximation of  $Q_{i,k}^a$  as

$$\begin{aligned} \hat{Q}_{i,k}^a(\mathbf{x}_{i,k}, \mathbf{u}_{i,k}) &\approx \hat{Q}_{i,k}^a(\bar{\mathbf{x}}_{i,k}, \bar{\mathbf{u}}_{i,k}) + \hat{Q}_{i,k}^{a,\top} \delta \mathbf{x}_{i,k} \\ &\quad + \hat{Q}_{i,k}^{a,\top} \delta \mathbf{u}_{i,k} + \frac{1}{2} \delta \mathbf{x}_{i,k}^\top \hat{Q}_{i,k}^a \delta \mathbf{x}_{i,k} \\ &\quad + \delta \mathbf{x}_{i,k}^\top \hat{Q}_{i,k}^a \delta \mathbf{u}_{i,k} \\ &\quad + \frac{1}{2} \delta \mathbf{u}_{i,k}^\top \hat{Q}_{i,k}^a \delta \mathbf{u}_{i,k}, \end{aligned} \quad (15)$$

with

$$\hat{Q}_{i,k}^a = \hat{\ell}_{i,k}^a + \mathbf{f}_{i,k}^\top \hat{V}_{i,k+1}^a, \quad (16a)$$

$$\hat{Q}_{i,k}^a = \hat{\ell}_{i,k}^a + \mathbf{f}_{i,k}^\top \hat{V}_{i,k+1}^a, \quad (16b)$$

$$\hat{Q}_{i\mathbf{x}_i,k}^a = \hat{\ell}_{i\mathbf{x}_i,k}^a + \mathbf{f}_{i,k}^\top \hat{V}_{i\mathbf{x}_i,k+1}^a \mathbf{f}_{i,k} + \hat{V}_{i\otimes,k+1}^a \mathbf{f}_{i\mathbf{x}_i,k} \quad (16c)$$

$$\hat{Q}_{i\mathbf{x}_i\mathbf{u}_i,k}^a = \hat{\ell}_{i\mathbf{x}_i\mathbf{u}_i,k}^a + \mathbf{f}_{i,k}^\top \hat{V}_{i\mathbf{x}_i\mathbf{u}_i,k+1}^a \mathbf{f}_{i,k} + \hat{V}_{i\otimes,k+1}^a \mathbf{f}_{i\mathbf{x}_i\mathbf{u}_i,k} \quad (16d)$$

$$\hat{Q}_{i\mathbf{u}_i\mathbf{u}_i,k}^a = \hat{\ell}_{i\mathbf{u}_i\mathbf{u}_i,k}^a + \mathbf{f}_{i,k}^\top \hat{V}_{i\mathbf{u}_i\mathbf{u}_i,k+1}^a \mathbf{f}_{i,k} + \hat{V}_{i\otimes,k+1}^a \mathbf{f}_{i\mathbf{u}_i\mathbf{u}_i,k} \quad (16e)$$

where  $\hat{V}_{i\otimes,k+1}^a := \hat{V}_{i\mathbf{x}_i\mathbf{x}_i,k+1}^{a,\top} \otimes \mathbf{I}$  with  $\otimes$  denoting the Kronecker product and  $\mathbf{I}$  the identity matrix of appropriate dimension. The notations  $(\cdot)_{\mathbf{x}_i} := \nabla_{\mathbf{x}_i}(\cdot)$ ,  $(\cdot)_{\mathbf{x}_i\mathbf{x}_i} := \nabla_{\mathbf{x}_i}^2(\cdot)$ , and  $(\cdot)_{\mathbf{x}_i\mathbf{u}_i} := \frac{\partial^2(\cdot)}{\partial \mathbf{x}_i \partial \mathbf{u}_i}$  apply similarly for  $\mathbf{u}_{i,k}$ . To avoid tensor computations, we define  $\mathbf{f}_{i\mathbf{x}_i\mathbf{x}_i,k} := \frac{\partial \text{vec}(\mathbf{f}_{i\mathbf{x}_i,k})}{\partial \mathbf{x}_i}$ . All the derivatives are



evaluated at the nominal trajectories. The last terms in (16c)-(16e) involve second-order derivatives of system dynamics. If omitted, DDP reduces to iterative LQR (iLQR) [62].

The optimal control deviation is obtained by minimizing the quadratic approximation (15):

$$\delta \mathbf{u}_{i,k}^* = \hat{\mathbf{K}}_{i,k}^a \delta \mathbf{x}_{i,k} + \hat{\mathbf{k}}_{i,k}^a, \quad (17)$$

where  $\hat{\mathbf{K}}_{i,k}^a = -\hat{\mathbf{Q}}_{\mathbf{u}_i \mathbf{u}_i, k}^{a,-1} \hat{\mathbf{Q}}_{\mathbf{x}_i \mathbf{u}_i, k}^{a,\top}$  and  $\hat{\mathbf{k}}_{i,k}^a = -\hat{\mathbf{Q}}_{\mathbf{u}_i \mathbf{u}_i, k}^{a,-1} \hat{\mathbf{Q}}_{\mathbf{u}_i, k}^a$  denote the feedback and feedforward gains, respectively. Plugging  $\delta \mathbf{u}_{i,k}^*$  into (15) and matching the resulting approximation  $\hat{\mathbf{Q}}_{i,k}^{a,*}$  with the second-order Taylor expansion of  $\hat{V}_{i,k}^a$  yields the following recursive updates:

$$\hat{V}_{\mathbf{x}_i, k}^a = \hat{\mathbf{Q}}_{\mathbf{x}_i, k}^a - \hat{\mathbf{Q}}_{\mathbf{x}_i \mathbf{u}_i, k}^a \hat{\mathbf{Q}}_{\mathbf{u}_i \mathbf{u}_i, k}^{a,-1} \hat{\mathbf{Q}}_{\mathbf{u}_i, k}^a, \quad (18a)$$

$$\hat{V}_{\mathbf{x}_i \mathbf{x}_i, k}^a = \hat{\mathbf{Q}}_{\mathbf{x}_i \mathbf{x}_i, k}^a - \hat{\mathbf{Q}}_{\mathbf{x}_i \mathbf{u}_i, k}^a \hat{\mathbf{Q}}_{\mathbf{u}_i \mathbf{u}_i, k}^{a,-1} \hat{\mathbf{Q}}_{\mathbf{x}_i \mathbf{u}_i, k}^{a,\top}, \quad (18b)$$

with the terminal derivatives as  $\hat{V}_{\mathbf{x}_i, N}^a = \hat{\ell}_{\mathbf{x}_i, N}^a$  and  $\hat{V}_{\mathbf{x}_i \mathbf{x}_i, N}^a = \hat{\ell}_{\mathbf{x}_i \mathbf{x}_i, N}^a$ . After computing these derivatives (16a)-(18b) backward in time, the nominal trajectories  $\{\bar{\mathbf{x}}_i, \bar{\mathbf{u}}_i\}$  are updated through the following forward iterations:

$$\mathbf{u}_{i,k} = \bar{\mathbf{u}}_{i,k} + \hat{\mathbf{K}}_{i,k}^a (\mathbf{x}_{i,k} - \bar{\mathbf{x}}_{i,k}) + \hat{\mathbf{k}}_{i,k}^a, \quad (19a)$$

$$\mathbf{x}_{i,k+1} = \mathbf{f}_i(\mathbf{x}_{i,k}, \mathbf{u}_{i,k}), \quad \mathbf{x}_{i,0} : \text{given}, \quad (19b)$$

$$\bar{\mathbf{x}}_{i,k} \leftarrow \mathbf{x}_{i,k}, \quad (19c)$$

$$\bar{\mathbf{u}}_{i,k} \leftarrow \mathbf{u}_{i,k}. \quad (19d)$$

The above backward and forward iterations are repeated until convergence, typically determined by a stopping condition such as  $\|\delta \mathbf{u}_{i,k}^*\|_2 \leq \epsilon$ , where  $\epsilon > 0$  is a predefined tolerance.

Finally, the distributed ADMM-DDP pipeline is summarized in Algorithm 1, where Subproblem 2 can be solved using a generic nonlinear programming method such as `ipopt` [63].

---

**Algorithm 1:** Distributed ADMM-DDP Pipeline

---

**Input:**  $\{\tilde{\mathbf{x}}_i^0, \tilde{\mathbf{u}}_i^0\}_{i=1}^n$ ,  $\{\lambda_i^0, \xi_i^0\}_{i=1}^n$ , and  $a = 0$ .

```

1 while ADMM not converged do
2   ▷ Subproblem 1
3   for  $i \leftarrow 1$  to  $n$  do
4      $\{\mathbf{x}_i^*, \mathbf{u}_i^*\}^{a+1} \leftarrow$  Solve (7) using DDP;
5   end for
6   ▷ Subproblem 2
7   for  $k \leftarrow 0$  to  $N-1$  do
8      $\{\tilde{\mathbf{x}}_k^*, \tilde{\mathbf{u}}_k^*\}^{a+1} \leftarrow$  Solve (9);
9   end for
10   $\tilde{\mathbf{x}}_N^{*,a+1} \leftarrow$  Solve (10);
11  ▷ Subproblem 3
12  for  $i \leftarrow 1$  to  $n$  do
13    for  $k \leftarrow 0$  to  $N-1$  do
14       $\{\lambda_{i,k}, \xi_{i,k}\}^{a+1} \leftarrow$  Solve (11a) and (11b);
15    end for
16     $\lambda_{i,N}^{a+1} \leftarrow$  Solve (11a);
17  end for
18   $a \leftarrow a + 1$ 
19 end while
Output:  $\{\mathbf{x}_i^{*,a}, \mathbf{u}_i^{*,a}\}_{i=1}^n$  and  $\{\tilde{\mathbf{x}}_i^{*,a}, \tilde{\mathbf{u}}_i^{*,a}\}_{i=1}^n$ .

```

---

### III. L2C: META-TRAJECTORY OPTIMIZATION

The quality of the trajectories optimized by the distributed ADMM-DDP (outlined in Algorithm 1) depends on a set of hyperparameters. In this section, we present the proposed L2C framework, which meta-learns these hyperparameters to enable generalization across diverse tasks.

#### A. Problem Statement

The trajectory quality in multiagent systems is typically evaluated by task fulfillment and inter-agent coordination. In the ADMM-DDP pipeline, the former is enforced through each agent's dynamics, costs, and constraints. For example, given a quadratic local cost:

$$\ell_{i,k} = \frac{1}{2} \|\mathbf{x}_{i,k} - \mathbf{x}_{i,k}^{\text{ref}}\|_{\mathbf{Q}_i}^2 + \frac{1}{2} \|\mathbf{u}_{i,k} - \mathbf{u}_{i,k}^{\text{ref}}\|_{\mathbf{R}_i}^2, \quad (20)$$

with  $\mathbf{Q}_i \succ 0$  and  $\mathbf{R}_i \succ 0$ , the trajectories are shaped by the reference waypoints  $\boldsymbol{\theta}_i^{\text{r}} := [\mathbf{x}_{i,k}^{\text{ref}}]_{k=0}^N$ , and the weights  $\boldsymbol{\theta}_i^{\text{w}} := [\text{vec}(\mathbf{Q}_i), \text{vec}(\mathbf{R}_i)]$  that balance waypoint tracking accuracy and control effort, with  $\text{vec}(\cdot)$  denoting the vectorization of a matrix. Additional influence arises from the system parameters  $\boldsymbol{\theta}_i^{\text{s}}$  in the dynamics  $\mathbf{f}_i$  and the constraint parameters  $\boldsymbol{\theta}_i^{\text{c}}$  such as safe margins for obstacle avoidance. Inter-agent coordination is governed by the ADMM penalty parameters  $[\rho_i]_{i=1}^n$ , which regulate consensus, and by the inter-agent constraint parameters  $\boldsymbol{\theta}_i^{\text{ic}}$  such as safe separation thresholds.

These hyperparameters interact nonlinearly. For instance, as shown in (8), a large  $\rho_i$  strengthens the consensus but can degrade the waypoint tracking if unbalanced with  $\boldsymbol{\theta}_i^{\text{w}}$ . Such coupling makes tuning difficult, especially with many agents or strong interactions. Manual tuning, based on intuition and trial-and-error, is inefficient and task-specific. Since dynamics, environments, and goals vary across tasks, the hyperparameters must adapt accordingly. To address this, we propose L2C, a general framework that meta-learns these hyperparameters for generalization across diverse task settings and agent counts.

#### B. Neural Adaptive Hyperparameters

For clarity, we aggregate each agent's hyperparameters into the vector  $\boldsymbol{\theta}_i = [\boldsymbol{\theta}_i^{\text{r}}, \boldsymbol{\theta}_i^{\text{w}}, \boldsymbol{\theta}_i^{\text{s}}, \boldsymbol{\theta}_i^{\text{c}}, \boldsymbol{\theta}_i^{\text{ic}}, \rho_i] \in \mathbb{R}^{p_i}$ , and define the total hyperparameter vector for the entire multiagent system as  $\boldsymbol{\theta} = [\boldsymbol{\theta}_1, \dots, \boldsymbol{\theta}_n] \in \mathbb{R}^{\sum p_i}$ .

To efficiently adapt the hyperparameters to diverse tasks, we model them using agent-wise neural networks:

$$\boldsymbol{\theta}_i = \pi_i(\boldsymbol{\chi}_i), \quad (21)$$

where  $\boldsymbol{\chi}_i$  is the network input, possibly including task-specific signals. Compared to a single large network for  $\boldsymbol{\theta}$ , the agent-wise design scales better with the number of agents. Isomorphic agents can also share one network, as shown in our simulations, further enhancing scalability.

#### C. Meta-Learning Via Gradient Descent

With the neural networks providing adaptability, the hyperparameter tuning becomes meta-learning the network parameters

$\varpi_{i=1}^n$  that perform well on average across multiple tasks. This can be cast as the following bi-level optimization problem:

$$\min_{\{\varpi_i\}_{i=1}^n} L := \frac{1}{M} \sum_{t=1}^M L_t(\{\tau_{i,t}^*, \tilde{\tau}_{i,t}^*\}_{i=1}^n) \quad (22a)$$

$$\text{s.t. } \theta_{i,t} = \pi_i(\chi_{i,t}), \forall i \in \{1, \dots, n\}, \quad (22b)$$

$$\{\tau_{i,t}^*, \tilde{\tau}_{i,t}^*\}_{i=1}^n \text{ generated by Algorithm 1.} \quad (22c)$$

Here,  $\tau_{i,t=1}^n = \{x_{i,t}^*, u_{i,t}^*\}_{i=1}^n$  and  $\tilde{\tau}_{i,t=1}^n = \{\tilde{x}_{i,t}^*, \tilde{u}_{i,t}^*\}_{i=1}^n$  denote the optimal trajectories of the original and copied variables of agent  $i$  in task  $t$ . The upper-level loss  $L_t$  evaluates these trajectories, generated by the lower-level problem (Algorithm 1) with the neural adaptive hyperparameters (22b). It captures both task fulfillment and inter-agent coordination, with the latter measured by ADMM residuals (consensus violations between the original and copied variables).

We aim to solve the bi-level optimization problem (22) via gradient descent. We compute the trajectory gradients w.r.t. all the hyperparameters jointly and then extract the relevant block for each agent:

$$\frac{dL}{d\varpi_i} = \frac{1}{M} \sum_{t=1}^M \left[ \sum_{i=1}^n \left( \frac{\partial L_t}{\partial \tau_{i,t}^*} \frac{d\tau_{i,t}^*}{d\theta} + \frac{\partial L_t}{\partial \tilde{\tau}_{i,t}^*} \frac{d\tilde{\tau}_{i,t}^*}{d\theta} \right) \right]_i \frac{\partial \theta_{i,t}}{\partial \varpi_i}, \quad (23)$$

where  $[\cdot]_i$  is the extraction of the block for agent  $i$ , using a selector matrix of the form  $[\dots, \mathbf{I}_{p_i}, \dots]$  with  $\mathbf{I}_{p_i} \in \mathbb{R}^{p_i \times p_i}$ .

Fig. 2 illustrates the L2C pipeline with two passes. In the forward pass, given  $\{\varpi_i\}_{i=1}^n$ , the neural networks output the adaptive hyperparameters, which the ADMM-DDP pipeline uses to generate optimal trajectories  $\{\tau_i^*, \tilde{\tau}_i^*\}_{i=1}^n$ . These trajectories are then evaluated to compute the loss (22a). In the backward pass, the gradients  $\{\frac{\partial L}{\partial \tau_i^*}, \frac{\partial L}{\partial \tilde{\tau}_i^*}\}_{i=1}^n$ ,  $\{\frac{d\tau_i^*}{d\theta}, \frac{d\tilde{\tau}_i^*}{d\theta}\}_{i=1}^n$ , and  $\{\frac{\partial \theta_{i,t}}{\partial \varpi_i}\}_{i=1}^n$  are computed for gradient descent.

Among these gradients,  $\{\frac{\partial L}{\partial \tau_{i,t}^*}, \frac{\partial L}{\partial \tilde{\tau}_{i,t}^*}\}_{i=1}^n$  are straightforward to compute since  $L$  is typically explicit in  $\{\tau_{i,t}^*, \tilde{\tau}_{i,t}^*\}_{i=1}^n$ . Computing  $\{\frac{\partial \theta_{i,t}}{\partial \varpi_i}\}_{i=1}^n$  is also standard and handled by automatic differentiation. The main challenge lies in  $\{\frac{d\tau_{i,t}^*}{d\theta}, \frac{d\tilde{\tau}_{i,t}^*}{d\theta}\}_{i=1}^n$ , which require differentiating through the full ADMM-DDP pipeline. Unlike single-agent settings [31], [35], these gradients must additionally satisfy the consensus and inter-agent constraints, making the multiagent gradient computation substantially harder. Nevertheless, we will show that they can be computed efficiently via an auxiliary ADMM-LQR system that reuses many intermediate results from the forward pass.

#### IV. ADMM-LQR DISTRIBUTED GRADIENT SOLVER

We aim to efficiently compute  $\{\frac{d\tau_{i,t}^*}{d\theta}, \frac{d\tilde{\tau}_{i,t}^*}{d\theta}\}_{i=1}^n$ . Recall from Section II that the ADMM-DDP pipeline comprises three subsystems for the dynamic optimization and the consensus enforcement. Here, we show that an auxiliary ADMM framework with the same three-subsystem structure can compute and coordinate these trajectory gradients efficiently.

##### A. Efficient Gradient Computation Via DDP Reuse

We begin with Subsystem 1 to solve for the DDP gradients. At ADMM iteration  $a$ , once DDP converges, each agent's

trajectory  $\tau_i^{*,a+1}$  satisfies the first-order optimality conditions given  $\theta$ . These conditions can be differentiated using the implicit function theorem (IFT) (Theorem 1B.1, [64]). A direct IFT application to the full trajectory, however, scales poorly with the horizon length  $N$  and is impractical for long-horizon planning. State-of-the-art methods such as PDP [35] and its variants [36], [37] avoid this by computing gradients recursively with linear complexity  $\mathcal{O}(N)$ . Our method preserves this  $\mathcal{O}(N)$  efficiency while further reducing runtime by reusing intermediate results from the forward DDP solve.

When DDP converges to a local optimum, the following optimality condition holds theoretically:

$$\mathbf{0} = \hat{Q}_{u_i,k}^{*,a}(\mathbf{x}_{i,k}^{*,a+1}, \mathbf{u}_{i,k}^{*,a+1}, \tilde{\mathbf{u}}_{i,k}^{*,a}, \boldsymbol{\xi}_{i,k}^a, \theta), \quad (24)$$

where  $(\cdot)^*$  indicates that the quantity is evaluated at the optimal solution. This follows from the standard DDP stopping criterion  $\|\delta \mathbf{u}_{i,k}^*\| \leq \epsilon$  (Section II), and can also be derived by differentiating (12) w.r.t.  $\mathbf{u}_{i,k}^{*,a+1}$ . Differentiating (12) w.r.t.  $\mathbf{x}_{i,k}^{*,a+1}$  yields the other optimality condition:

$$\hat{V}_{x_i,k}^a = \hat{Q}_{x_i,k}^{*,a}(\mathbf{x}_{i,k}^{*,a+1}, \mathbf{u}_{i,k}^{*,a+1}, \tilde{\mathbf{x}}_{i,k}^{*,a}, \boldsymbol{\lambda}_{i,k}^a, \theta). \quad (25)$$

Finally, the optimal state and control input satisfy the agent's dynamics (1b):

$$\mathbf{x}_{i,k+1}^{*,a+1} = \mathbf{f}_i(\mathbf{x}_{i,k}^{*,a+1}, \mathbf{u}_{i,k}^{*,a+1}, \theta). \quad (26)$$

The equations (24), (25), and (26) constitute the first-order optimality conditions for Subsystem 1 (7).

Recall that our goal is to solve for  $\frac{d\tau_i^*}{d\theta}$ . We are motivated to implicitly differentiate both sides of (25), (24), and (26) w.r.t.  $\theta$  using chain rule. This yields the following differential optimality conditions for Subsystem 1:

$$\frac{d\hat{V}_{x_i,k}^a}{d\theta} = \hat{Q}_{x_i x_i,k}^{*,a} \frac{d\mathbf{x}_{i,k}^{*,a+1}}{d\theta} + \hat{Q}_{x_i u_i,k}^{*,a} \frac{d\mathbf{u}_{i,k}^{*,a+1}}{d\theta} + \hat{Q}_{x_i \theta,k}^{*,a}, \quad (27a)$$

$$\mathbf{0} = \hat{Q}_{u_i x_i,k}^{*,a} \frac{d\mathbf{x}_{i,k}^{*,a+1}}{d\theta} + \hat{Q}_{u_i u_i,k}^{*,a} \frac{d\mathbf{u}_{i,k}^{*,a+1}}{d\theta} + \hat{Q}_{u_i \theta,k}^{*,a}, \quad (27b)$$

$$\frac{d\mathbf{x}_{i,k+1}^{*,a+1}}{d\theta} = \mathbf{f}_{x_i,k}^* \frac{d\mathbf{x}_{i,k}^{*,a+1}}{d\theta} + \mathbf{f}_{u_i,k}^* \frac{d\mathbf{u}_{i,k}^{*,a+1}}{d\theta} + \mathbf{f}_{\theta,k}^*, \quad (27c)$$

where  $\hat{Q}_{x_i x_i,k}^{*,a}$ ,  $\hat{Q}_{x_i u_i,k}^{*,a}$ , and  $\hat{Q}_{u_i u_i,k}^{*,a}$  are defined in (16c), (16d), and (16e), respectively, but are evaluated at the optimal solutions,  $\hat{Q}_{u_i x_i,k}^{*,a} = \hat{Q}_{x_i u_i,k}^{*,a\top}$ , and  $\mathbf{f}_{\theta,k}^* = \nabla_{\theta} \mathbf{f}_i$ .

Note that the last terms  $\hat{Q}_{x_i \theta,k}^{*,a}$  and  $\hat{Q}_{u_i \theta,k}^{*,a}$  in (27a) and (27b) not only represent the partial derivatives of  $\hat{Q}_{x_i,k}^{*,a}$  (16a) and  $\hat{Q}_{u_i,k}^{*,a}$  (16b) w.r.t.  $\theta$ , but also incorporate the gradients of  $\tilde{\mathbf{x}}_{i,k}^{*,a}$ ,  $\tilde{\mathbf{u}}_{i,k}^{*,a}$ ,  $\boldsymbol{\lambda}_{i,k}^a$ , and  $\boldsymbol{\xi}_{i,k}^a$  w.r.t.  $\theta$ , leading to

$$\hat{Q}_{x_i \theta,k}^{*,a} = \nabla_{\theta} \hat{Q}_{x_i,k}^{*,a} + \hat{Q}_{x_i \tilde{x}_i,k}^{*,a} \frac{d\tilde{\mathbf{x}}_{i,k}^{*,a}}{d\theta} + \hat{Q}_{x_i \boldsymbol{\lambda}_i,k}^{*,a} \frac{d\boldsymbol{\lambda}_{i,k}^a}{d\theta}, \quad (28a)$$

$$\hat{Q}_{u_i \theta,k}^{*,a} = \nabla_{\theta} \hat{Q}_{u_i,k}^{*,a} + \hat{Q}_{u_i \tilde{u}_i,k}^{*,a} \frac{d\tilde{\mathbf{u}}_{i,k}^{*,a}}{d\theta} + \hat{Q}_{u_i \boldsymbol{\xi}_i,k}^{*,a} \frac{d\boldsymbol{\xi}_{i,k}^a}{d\theta}. \quad (28b)$$

From the augmented Lagrangian (6), the partial derivatives are directly obtained as  $\hat{Q}_{x_i \tilde{x}_i,k}^{*,a} = -\rho_i \mathbf{I}_{n_i}$ ,  $\hat{Q}_{x_i \boldsymbol{\lambda}_i,k}^{*,a} = \mathbf{I}_{n_i}$ ,  $\hat{Q}_{u_i \tilde{u}_i,k}^{*,a} = -\rho_i \mathbf{I}_{m_i}$ , and  $\hat{Q}_{u_i \boldsymbol{\xi}_i,k}^{*,a} = \mathbf{I}_{m_i}$ . The gradients  $\frac{d\tilde{\tau}_{i,t}^{*,a}}{d\theta}$

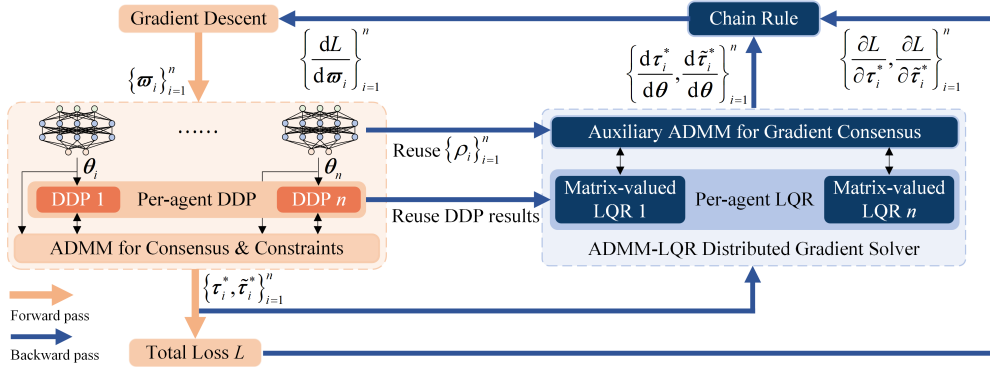


Fig. 2: The L2C learning pipeline. In the forward pass, the agents' optimal trajectories  $\{\tau_i^*, \tilde{\tau}_i^*\}_{i=1}^n$  are generated by the ADMM-DDP pipeline 1 using the neural adaptive hyperparameters (21). In the backward pass, central to L2C is the ADMM-LQR distributed gradient solver, which analytically computes and coordinates the agent-wise gradients for meta-learning. A key insight is that this solver can be constructed and solved efficiently by reusing many of the key intermediate results from the forward pass.

and  $\{\frac{d\lambda_{i,k}^a}{d\theta}, \frac{d\xi_{i,k}^a}{d\theta}\}$  are computed in Subsystems 2 and 3 at the previous ADMM iteration  $a - 1$ . Thus, gradient computations across subsystems are inherently coupled, posing a major challenge and fundamentally distinguishing the multiagent case from its single-agent counterpart. We show that these gradient couplings can be efficiently coordinated through an auxiliary ADMM framework. In this subsection, we focus on computing  $\frac{d\tau_{i,a+1}^*}{d\theta}$ , assuming  $\frac{d\tilde{\tau}_i^*}{d\theta}$  and  $\{\frac{d\lambda_i^a}{d\theta}, \frac{d\xi_i^a}{d\theta}\}$  are already available. With sufficient ADMM iterations, these gradients  $\frac{d\tau_{i,a+1}^*}{d\theta}$  converge to their optimal values  $\frac{d\tau_i^*}{d\theta}$ .

We refer to the conditions (27a), (27b), and (27c) as the differential Bellman's principle (DBP) conditions. Interestingly, the DBP conditions are equivalent to the differential PMP conditions, upon which the PDP method constructs an auxiliary matrix-valued LQR control system to recursively compute the gradients (Lemma 5.1 in [35]). Our key insight is that the same LQR system can also be built from DBP, as formalized in the following lemma.

**Lemma 1.** Consider a generic dynamic optimization problem:

$$\min_{\mathbf{x}, \mathbf{u}} \sum_{k=0}^{N-1} \ell_k(\mathbf{x}_k, \mathbf{u}_k, \boldsymbol{\theta}) + \ell_N(\mathbf{x}_N, \boldsymbol{\theta}) \quad (29)$$

s.t.  $\mathbf{x}_{k+1} = \mathbf{f}_k(\mathbf{x}_k, \mathbf{u}_k, \boldsymbol{\theta})$ ,  $\mathbf{x}_0$  : given,

where  $\mathbf{x}_k \in \mathbb{R}^n$ ,  $\mathbf{u}_k \in \mathbb{R}^m$ , and  $\boldsymbol{\theta} \in \mathbb{R}^p$  are the state, control, and hyperparameters. Let its Bellman's principle be defined as  $V_k(\mathbf{x}_k, \boldsymbol{\theta}) = \min_{\mathbf{u}_k} Q(\mathbf{x}_k, \mathbf{u}_k, \boldsymbol{\theta})$ , and its PMP Hamiltonian as  $\mathcal{H}_k = \ell_k + \boldsymbol{\lambda}_{k+1}^\top \mathbf{f}_k$  where  $\boldsymbol{\lambda}_k \in \mathbb{R}^n$  is the co-state. The DBP conditions follow directly from (27) after specializing to the single-agent case. By the relation  $\boldsymbol{\lambda}_k^* = \nabla_{\mathbf{x}_k} V_k$ , these DBP conditions are equivalent to the differential PMP conditions:

$$\frac{d\boldsymbol{\lambda}_k^*}{d\boldsymbol{\theta}} = H_{\mathbf{x}\mathbf{x},k}^* \frac{d\mathbf{x}_k^*}{d\boldsymbol{\theta}} + H_{\mathbf{x}\mathbf{u},k}^* \frac{d\mathbf{u}_k^*}{d\boldsymbol{\theta}} + \mathbf{f}_{\mathbf{x},k}^{*\top} \frac{d\boldsymbol{\lambda}_{k+1}^*}{d\boldsymbol{\theta}} + H_{\mathbf{x}\boldsymbol{\theta},k}^*, \quad (30a)$$

$$\mathbf{0} = H_{\mathbf{u}\mathbf{x},k}^* \frac{d\mathbf{x}_k^*}{d\boldsymbol{\theta}} + H_{\mathbf{u}\mathbf{u},k}^* \frac{d\mathbf{u}_k^*}{d\boldsymbol{\theta}} + \mathbf{f}_{\mathbf{u},k}^{*\top} \frac{d\boldsymbol{\lambda}_{k+1}^*}{d\boldsymbol{\theta}} + H_{\mathbf{u}\boldsymbol{\theta},k}^*, \quad (30b)$$

$$\frac{d\mathbf{x}_{k+1}^*}{d\boldsymbol{\theta}} = \mathbf{f}_{\mathbf{x},k}^* \frac{d\mathbf{x}_k^*}{d\boldsymbol{\theta}} + \mathbf{f}_{\mathbf{u},k}^* \frac{d\mathbf{u}_k^*}{d\boldsymbol{\theta}} + \mathbf{f}_{\boldsymbol{\theta},k}^*. \quad (30c)$$

From (30), the following matrix-valued LQR system is built:

$$\begin{aligned} \min_{\mathbf{X}, \mathbf{U}} \bar{J} := & \sum_{k=0}^{N-1} \text{tr} \left( \frac{1}{2} \begin{bmatrix} \mathbf{X}_k \\ \mathbf{U}_k \end{bmatrix}^\top \begin{bmatrix} H_{\mathbf{x}\mathbf{x},k}^* & H_{\mathbf{x}\mathbf{u},k}^* \\ H_{\mathbf{u}\mathbf{x},k}^* & H_{\mathbf{u}\mathbf{u},k}^* \end{bmatrix} \begin{bmatrix} \mathbf{X}_k \\ \mathbf{U}_k \end{bmatrix} \right. \\ & \left. + \begin{bmatrix} H_{\mathbf{x}\boldsymbol{\theta},k}^* \\ H_{\mathbf{u}\boldsymbol{\theta},k}^* \end{bmatrix}^\top \begin{bmatrix} \mathbf{X}_k \\ \mathbf{U}_k \end{bmatrix} \right) \\ & + \text{tr} \left( \frac{1}{2} \mathbf{X}_N^\top H_{\mathbf{x}\mathbf{x},N}^* \mathbf{X}_N + H_{\mathbf{x}\boldsymbol{\theta},N}^{*\top} \mathbf{X}_N \right) \end{aligned} \quad (31)$$

$$\text{s.t. } \mathbf{X}_{k+1} = \mathbf{f}_{\mathbf{x},k}^* \mathbf{X}_k + \mathbf{f}_{\mathbf{u},k}^* \mathbf{U}_k + \mathbf{f}_{\boldsymbol{\theta},k}^* \text{ with } \mathbf{X}_0 = \mathbf{0},$$

where  $\mathbf{X}_k \in \mathbb{R}^{n \times p}$  and  $\mathbf{U}_k \in \mathbb{R}^{m \times p}$  are the matrix-valued state and control, respectively, and  $\text{tr}(\cdot)$  is the matrix trace operator. Denote its optimal solutions by  $\{\mathbf{X}_{0:N}^*, \mathbf{U}_{0:N-1}^*\}$ . These solutions satisfy Bellman's principle of (31), which coincides with the DBP conditions (27). Consequently,

$$\{\mathbf{X}_{0:N}^*, \mathbf{U}_{0:N-1}^*\} = \left\{ \frac{d\mathbf{x}_{0:N}^*}{d\boldsymbol{\theta}}, \frac{d\mathbf{u}_{0:N-1}^*}{d\boldsymbol{\theta}} \right\}. \quad (32)$$

*Proof.* See Appendix-A.  $\square$

Lemma 1 shows that the required gradients can be obtained analytically by solving (31). Importantly, when DDP is used for dynamic optimization, the Hessians  $\{H_{\mathbf{x}\mathbf{x},k}^*\}_{k=0}^N$ ,  $\{H_{\mathbf{x}\mathbf{u},k}^*\}_{k=0}^{N-1}$ , and  $\{H_{\mathbf{u}\mathbf{u},k}^*\}_{k=0}^{N-1}$ , together with the Jacobians  $\{\mathbf{f}_{\mathbf{x},k}^*, \mathbf{f}_{\mathbf{u},k}^*\}_{k=0}^{N-1}$ , are already available from the DDP derivatives (16) and can be reused to construct (31). Unlike PDP [35], which solves (31) via PMP conditions, we exploit Bellman's principle to preserve  $\mathcal{O}(N)$ . Moreover, by reusing key DDP intermediates such as Riccati recursions  $V_{\mathbf{x}\mathbf{x},k}$  and feedback gains  $\mathbf{K}_k$ , our approach achieves higher efficiency in the gradient computation, as formalized in the following lemma.

**Lemma 2.** Let  $\{Q_{\mathbf{u}\mathbf{u},k}^*, Q_{\mathbf{x}\mathbf{u},k}^*, \mathbf{f}_{\mathbf{x},k}^*, \mathbf{f}_{\mathbf{u},k}^*, \mathbf{K}_k, V_{\mathbf{x}\mathbf{x},k+1}\}_{k=0}^{N-1}$  denote the quantities computed during the DDP solve for Problem (29). Then, the following Riccati equation can be solved efficiently backward in time from  $k = N - 1$  to  $k = 0$ :

$$\begin{aligned} V_{\mathbf{x}\boldsymbol{\theta},k} = & H_{\mathbf{x}\boldsymbol{\theta},k}^* + \mathbf{f}_{\mathbf{x},k}^{*\top} V_{\mathbf{x}\boldsymbol{\theta},k+1} + \mathbf{f}_{\mathbf{x},k}^{*\top} V_{\mathbf{x}\mathbf{x},k+1} \mathbf{f}_{\boldsymbol{\theta},k}^* \\ & - Q_{\mathbf{x}\mathbf{u},k}^* Q_{\mathbf{u}\mathbf{u},k}^{*-1} \left( H_{\mathbf{u}\boldsymbol{\theta},k}^* + \mathbf{f}_{\mathbf{u},k}^{*\top} V_{\mathbf{x}\boldsymbol{\theta},k+1} \right. \\ & \left. + \mathbf{f}_{\mathbf{u},k}^{*\top} V_{\mathbf{x}\mathbf{x},k+1} \mathbf{f}_{\boldsymbol{\theta},k}^* \right), \end{aligned} \quad (33)$$

with the terminal condition  $V_{\mathbf{x}\theta,N} = H_{\mathbf{x}\theta,N}^* = \ell_{\mathbf{x}\theta,N}^*$ . Define the feedforward gain

$$\mathbf{K}_k^{\text{ff}} := -Q_{\mathbf{u}\mathbf{u},k}^{*-1} \left( H_{\mathbf{u}\theta,k}^* + f_{\mathbf{u},k}^{*,\top} V_{\mathbf{x}\theta,k+1} + f_{\mathbf{u},k}^{*,\top} V_{\mathbf{x}\mathbf{x},k+1} f_{\theta,k}^* \right).$$

Then, the gradient trajectories  $\{\mathbf{X}_{0:N}^*, \mathbf{U}_{0:N-1}^*\}$  can be computed by the following forward recursion from  $k = 0$  to  $k = N - 1$ , with the initial condition  $\mathbf{X}_0^* = \mathbf{0}$ :

$$\mathbf{U}_k^* = \mathbf{K}_k \mathbf{X}_k^* + \mathbf{K}_k^{\text{ff}}, \quad (34a)$$

$$\mathbf{X}_{k+1}^* = f_{\mathbf{x},k}^* \mathbf{X}_k^* + f_{\mathbf{u},k}^* \mathbf{U}_k^* + f_{\theta,k}^*. \quad (34b)$$

*Proof.* See Appendix-B.  $\square$

The optimal matrix-valued control law (34a) shares a similar structure with the DDP control law (17). The feedback gain  $\mathbf{K}_k$  contributes to stabilizing the gradient computation. Moreover, the inverse  $Q_{\mathbf{u}\mathbf{u},k}^{*-1}$  is already computed during the DDP solve and can therefore be efficiently reused, avoiding redundant and costly matrix inversions. Lemma 2 applies to generic DDP problems. When using it to compute  $\frac{d\tau_{i,k}^{*,a+1}}{d\theta}$  for Subproblem 1 in (7), we must augment the terms  $H_{\mathbf{x}\theta,k}^*$  and  $H_{\mathbf{u}\theta,k}^*$  to incorporate the gradient contributions from Subproblem 2 and 3, as specified in (28). This results in the following expressions, which explicitly account for the gradient couplings:

$$\hat{H}_{\mathbf{x}\theta,k}^{*,a} = \nabla_{\theta} \hat{H}_{\mathbf{x},k}^{*,a} - \rho_i \frac{d\tilde{\mathbf{x}}_{i,k}^{*,a}}{d\theta} + \frac{d\lambda_{i,k}^a}{d\theta}, \quad (35a)$$

$$\hat{H}_{\mathbf{u}\theta,k}^{*,a} = \nabla_{\theta} \hat{H}_{\mathbf{u},k}^{*,a} - \rho_i \frac{d\tilde{\mathbf{u}}_{i,k}^{*,a}}{d\theta} + \frac{d\xi_{i,k}^a}{d\theta}. \quad (35b)$$

In aligning with (28), we use the hat notation  $\hat{(\cdot)}$  to indicate that the quantity  $(\cdot)$  includes the augmented cost (8).

### B. Gradient Coordination Via ADMM

This subsection constructs an auxiliary ADMM framework to enforce the gradient-matching constraints  $\{\frac{d\tau_i^*}{d\theta} = \frac{d\tilde{\tau}_i^*}{d\theta}\}_{i=1}^n$ , arising from the *safe-copy-variable* strategy (5). Each ADMM iteration mirrors the forward-pass pipeline and consists of three auxiliary subsystems that update  $\frac{d\tau_i^{*,a}}{d\theta}$ ,  $\frac{d\tilde{\tau}_i^{*,a}}{d\theta}$ , and  $\frac{d\lambda_{i,k}^a}{d\theta}$ ,  $\frac{d\xi_{i,k}^a}{d\theta}$ , respectively.

*Auxiliary Subsystem 1 (see Subsection IV-A):* Each agent obtains its DDP gradients  $\{\mathbf{X}_i^*, \mathbf{U}_i^*\}^{a+1}$  by solving the following auxiliary matrix-valued LQR subproblem using Lemma 2:

$$\begin{aligned} \min_{\mathbf{X}_i, \mathbf{U}_i} \bar{J}_i &:= \sum_{k=0}^{N-1} \text{tr} \left( \frac{1}{2} \begin{bmatrix} \mathbf{X}_{i,k} \\ \mathbf{U}_{i,k} \end{bmatrix}^\top \begin{bmatrix} \hat{H}_{\mathbf{x}\mathbf{x},k}^{*,a} & \hat{H}_{\mathbf{x}\mathbf{u},k}^{*,a} \\ \hat{H}_{\mathbf{u}\mathbf{x},k}^{*,a} & \hat{H}_{\mathbf{u}\mathbf{u},k}^{*,a} \end{bmatrix} \begin{bmatrix} \mathbf{X}_{i,k} \\ \mathbf{U}_{i,k} \end{bmatrix} \right. \\ &\quad \left. + \begin{bmatrix} \hat{H}_{\mathbf{x}\theta,k}^{*,a} \\ \hat{H}_{\mathbf{u}\theta,k}^{*,a} \end{bmatrix}^\top \begin{bmatrix} \mathbf{X}_{i,k} \\ \mathbf{U}_{i,k} \end{bmatrix} \right) \\ &\quad + \text{tr} \left( \frac{1}{2} \mathbf{X}_{i,N}^\top \hat{H}_{\mathbf{x}\mathbf{x},N}^{*,a} \mathbf{X}_{i,N} + \hat{H}_{\mathbf{x}\theta,N}^{*,a} \mathbf{X}_{i,N} \right) \\ \text{s.t. } \mathbf{X}_{i,k+1} &= f_{\mathbf{x},k}^* \mathbf{X}_{i,k} + f_{\mathbf{u},k}^* \mathbf{U}_{i,k} + f_{\theta,k}^* \text{ with } \mathbf{X}_{i,0} = \mathbf{0}, \end{aligned} \quad (36)$$

Here,  $\hat{H}_{\mathbf{x}\theta,k}^{*,a}$  and  $\hat{H}_{\mathbf{u}\theta,k}^{*,a}$  are defined in (35). The Hamiltonian  $\hat{\mathcal{H}}_{i,k}$  used to compute the Hessians  $\hat{H}_{(\cdot)(\cdot),k}^{*,a}$  is constructed using the augmented cost (8):

$$\begin{aligned} \hat{\mathcal{H}}_{i,k} &= \ell_{i,k} + \frac{\rho_i}{2} \left\| \mathbf{x}_{i,k}^{*,a+1} - \tilde{\mathbf{x}}_{i,k}^{*,a} + \frac{\lambda_{i,k}^a}{\rho_i} \right\|_2^2 \\ &\quad + \frac{\rho_i}{2} \left\| \mathbf{u}_{i,k}^{*,a+1} - \tilde{\mathbf{u}}_{i,k}^{*,a} + \frac{\xi_{i,k}^a}{\rho_i} \right\|_2^2 + V_{\mathbf{x},k+1}^\top \mathbf{f}_i, \end{aligned} \quad (37)$$

and all the Hessians are evaluated at the optimal solutions  $\{\mathbf{x}_k^{*,a+1}, \mathbf{u}_k^{*,a+1}, \tilde{\mathbf{x}}_k^{*,a}, \tilde{\mathbf{u}}_k^{*,a}, \lambda_k^a, \xi_k^a\}$ .

*Auxiliary Subsystem 2:* All agents compute the gradients of their safe-copy variables  $\{\frac{d\tilde{\mathbf{x}}_k^{*,a+1}}{d\theta}, \frac{d\tilde{\mathbf{u}}_k^{*,a+1}}{d\theta}\}$  by implicitly differentiating through the static optimization problems (9) and (10). These gradients correspond to the optimal solutions  $\{\tilde{\mathbf{X}}_k^{*,a+1}, \tilde{\mathbf{U}}_k^{*,a+1}\}$  of the following matrix-valued static optimization problems, derived using the IFT in a manner similar to the LQR subproblem (36).

At  $k = 0, \dots, N - 1$ , the stage-wise matrix-valued static optimization subproblem is formulated as:

$$\begin{aligned} \min_{\tilde{\mathbf{X}}_k, \tilde{\mathbf{U}}_k} \bar{J}_k &:= \text{tr} \left( \frac{1}{2} \begin{bmatrix} \tilde{\mathbf{X}}_k \\ \tilde{\mathbf{U}}_k \end{bmatrix}^\top \begin{bmatrix} \hat{L}_{\tilde{\mathbf{x}}\tilde{\mathbf{x}},k}^{*,a} & \hat{L}_{\tilde{\mathbf{x}}\tilde{\mathbf{u}},k}^{*,a} \\ \hat{L}_{\tilde{\mathbf{u}}\tilde{\mathbf{x}},k}^{*,a} & \hat{L}_{\tilde{\mathbf{u}}\tilde{\mathbf{u}},k}^{*,a} \end{bmatrix} \begin{bmatrix} \tilde{\mathbf{X}}_k \\ \tilde{\mathbf{U}}_k \end{bmatrix} \right. \\ &\quad \left. + \begin{bmatrix} \hat{L}_{\tilde{\mathbf{x}}\theta,k}^{*,a} \\ \hat{L}_{\tilde{\mathbf{u}}\theta,k}^{*,a} \end{bmatrix}^\top \begin{bmatrix} \tilde{\mathbf{X}}_k \\ \tilde{\mathbf{U}}_k \end{bmatrix} \right), \end{aligned} \quad (38)$$

where  $\hat{L}_{(\cdot)(\cdot),k}^{*,a} := \frac{\partial^2 \hat{\mathcal{L}}_k}{\partial(\cdot)\partial(\cdot)}$  denotes the Hessians of the approximated Lagrangian  $\hat{\mathcal{L}}_k$  of Subproblem (9), evaluated at the optimal solutions  $\{\mathbf{x}_k^{*,a+1}, \mathbf{u}_k^{*,a+1}, \tilde{\mathbf{x}}_k^{*,a+1}, \tilde{\mathbf{u}}_k^{*,a+1}, \lambda_k^a, \xi_k^a\}$ . The approximated Lagrangian  $\hat{\mathcal{L}}_k$  takes the following form:

$$\begin{aligned} \hat{\mathcal{L}}_k &= \sum_{i=1}^n \left( \frac{\rho_i}{2} \left\| \mathbf{x}_{i,k}^{*,a+1} - \tilde{\mathbf{x}}_{i,k}^{*,a+1} + \frac{\lambda_{i,k}^a}{\rho_i} \right\|_2^2 \right. \\ &\quad \left. + \frac{\rho_i}{2} \left\| \mathbf{u}_{i,k}^{*,a+1} - \tilde{\mathbf{u}}_{i,k}^{*,a+1} + \frac{\xi_{i,k}^a}{\rho_i} \right\|_2^2 \right) \\ &\quad - \mu \sum_{i=1}^n \left[ \ln(-\mathbf{g}_{i,k}) + \sum_{j \neq i}^n \ln(-\mathbf{h}_{ij,k}) \right]. \end{aligned} \quad (39)$$

All constraints in (9) are approximated as soft constraints using logarithmic barrier functions, with  $\mu \in \mathbb{R}^+$  being the barrier parameter. This approximation renders the optimality conditions differentiable without identifying active inequalities (i.e.,  $\mathbf{g}_{i,k} = 0$ ,  $\mathbf{b}_{i,k} = 0$ ,  $\mathbf{h}_{ij,k} = 0$ ). It improves numerical stability by mitigating discontinuous switching between inactive and active sets, while also reducing computation by avoiding Lagrange multipliers for these constraints. This technique, explored in Safe-PDP, has shown stable and effective learning in MPC [36]. As  $\mu \rightarrow 0$ , we recover  $\tilde{\mathbf{X}}_k^{*,a+1} \rightarrow \frac{d\tilde{\mathbf{x}}_k^{*,a+1}}{d\theta}$  and  $\tilde{\mathbf{U}}_k^{*,a+1} \rightarrow \frac{d\tilde{\mathbf{u}}_k^{*,a+1}}{d\theta}$  (Theorem 2 in [36]).

At  $k = N$ , the terminal matrix-valued static optimization subproblem is given by:

$$\min_{\tilde{\mathbf{X}}_N} \bar{J}_N := \text{tr} \left( \frac{1}{2} \tilde{\mathbf{X}}_N^\top \hat{L}_{\tilde{\mathbf{x}}\tilde{\mathbf{x}},N}^{*,a} \tilde{\mathbf{X}}_N + \hat{L}_{\tilde{\mathbf{x}}\theta,N}^{*,a} \tilde{\mathbf{X}}_N \right), \quad (40)$$

where the approximated Lagrangian  $\hat{\mathcal{L}}_N$  used to compute the Hessians  $\hat{L}_{(\cdot)(\cdot),N}^{*,a}$  is also defined using the soft-constraint strategy as follows:

$$\hat{\mathcal{L}}_N = \sum_{i=1}^n \frac{\rho_i}{2} \left\| \mathbf{x}_{i,N}^{*,a+1} - \tilde{\mathbf{x}}_{i,N}^{*,a+1} + \frac{\boldsymbol{\lambda}_{i,N}^a}{\rho_i} \right\|_2^2 - \mu \sum_{i=1}^n \left[ \ln(-\mathbf{g}_{i,N}) + \sum_{j \neq i} \ln(-\mathbf{h}_{ij,N}) \right]. \quad (41)$$

Both (38) and (41) are unconstrained quadratic programming problems, which admit analytical solutions. Similar to (35), the terms  $L_{\tilde{\mathbf{x}}\boldsymbol{\theta},k}^{*,a}$  and  $L_{\tilde{\mathbf{u}}\boldsymbol{\theta},k}^{*,a}$  incorporate the coupling contributions from the gradients of  $\mathbf{x}_k^{*,a+1}$ ,  $\mathbf{u}_k^{*,a+1}$ ,  $\boldsymbol{\lambda}_k^a$ , and  $\boldsymbol{\xi}_k^a$  w.r.t.  $\boldsymbol{\theta}$ , leading to the following expressions:

$$\hat{L}_{\tilde{\mathbf{x}}\boldsymbol{\theta},k}^{*,a} = \nabla_{\boldsymbol{\theta}} \hat{L}_{\tilde{\mathbf{x}},k}^{*,a} + \hat{L}_{\tilde{\mathbf{x}},k}^{*,a} \frac{d\mathbf{x}_k^{*,a+1}}{d\boldsymbol{\theta}} + \hat{L}_{\tilde{\mathbf{x}},k}^{*,a} \frac{d\boldsymbol{\lambda}_k^a}{d\boldsymbol{\theta}}, \quad (42a)$$

$$\hat{L}_{\tilde{\mathbf{u}}\boldsymbol{\theta},k}^{*,a} = \nabla_{\boldsymbol{\theta}} \hat{L}_{\tilde{\mathbf{u}},k}^{*,a} + \hat{L}_{\tilde{\mathbf{u}},k}^{*,a} \frac{d\mathbf{u}_k^{*,a+1}}{d\boldsymbol{\theta}} + \hat{L}_{\tilde{\mathbf{u}},k}^{*,a} \frac{d\boldsymbol{\xi}_k^a}{d\boldsymbol{\theta}}, \quad (42b)$$

where  $\hat{L}_{\tilde{\mathbf{x}},k}^{*,a} = -\text{Blkdiag}[\rho_i \mathbf{I}_{n_i}]_{i=1}^n$ ,  $\hat{L}_{\tilde{\mathbf{x}},k}^{*,a} = -\mathbf{I}_{\sum n_i}$ ,  $\hat{L}_{\tilde{\mathbf{u}},k}^{*,a} = -\text{Blkdiag}[\rho_i \mathbf{I}_{m_i}]_{i=1}^n$ , and  $\hat{L}_{\tilde{\mathbf{u}},k}^{*,a} = -\mathbf{I}_{\sum m_i}$ , derived directly from (39) and (41). The gradients  $\frac{d\mathbf{x}_k^{*,a+1}}{d\boldsymbol{\theta}}$  and  $\frac{d\mathbf{u}_k^{*,a+1}}{d\boldsymbol{\theta}}$  are obtained from the optimal solutions  $\mathbf{X}_i^{*,a+1}$  and  $\mathbf{U}_i^{*,a+1}$  at time step  $k$  across all agents, by independently solving (36) for each agent, which can be done in parallel.

*Auxiliary Subsystem 3:* At each step, each agent independently updates the gradients of its dual variables,  $\frac{d\boldsymbol{\lambda}_{i,k}^a}{d\boldsymbol{\theta}}$  and  $\frac{d\boldsymbol{\xi}_{i,k}^a}{d\boldsymbol{\theta}}$ . Differentiating both sides of (11) w.r.t.  $\boldsymbol{\theta}$  yields:

$$\frac{d\boldsymbol{\lambda}_{i,k}^{a+1}}{d\boldsymbol{\theta}} = \frac{d\boldsymbol{\lambda}_{i,k}^a}{d\boldsymbol{\theta}} + \rho_i \left( \mathbf{X}_{i,k}^{*,a+1} - \tilde{\mathbf{X}}_{i,k}^{*,a+1} \right) + \nabla_{\boldsymbol{\theta}} \left[ \rho_i (\mathbf{x}_{i,k}^{a+1} - \tilde{\mathbf{x}}_{i,k}^{a+1}) \right], \quad (43a)$$

$$\frac{d\boldsymbol{\xi}_{i,k}^{a+1}}{d\boldsymbol{\theta}} = \frac{d\boldsymbol{\xi}_{i,k}^a}{d\boldsymbol{\theta}} + \rho_i \left( \mathbf{U}_{i,k}^{*,a+1} - \tilde{\mathbf{U}}_{i,k}^{*,a+1} \right) + \nabla_{\boldsymbol{\theta}} \left[ \rho_i (\mathbf{u}_{i,k}^{a+1} - \tilde{\mathbf{u}}_{i,k}^{a+1}) \right], \quad (43b)$$

where the last terms represent the explicit partial derivatives of the R.H.S. of (11a) and (11b) w.r.t.  $\rho_i^1$ .

Finally, the ADMM-LQR framework for the gradient computation is summarized in Algorithm 2. For consistency, it is run for the same number of ADMM iterations as the forward pass. At each iteration, the auxiliary subsystems (36), (38), and (40) are constructed using the optimal trajectories stored from Algorithm 1. Since we differentiate the entire ADMM-DDP pipeline, the ADMM-LQR-based gradient solver reuses  $\rho_i$  from the forward pass, as shown in (35), (42), and (43). It can be viewed as the distributed solution for a matrix-valued quadratic programming problem, as formalized in Lemma 3.

<sup>1</sup>They can be viewed as perturbations to the dual updates. Similar perturbed dual forms are reported in ADMM pipelines, e.g., to enhance privacy [65]. In (43), these perturbations are proportional to the ADMM residuals, which are assumed to decrease and remain bounded as iterations progress. They vanish when either  $\rho_i \notin \boldsymbol{\theta}$  or the primal residuals converge to zero.

---

**Algorithm 2:** ADMM-LQR-based Gradient Solver

---

**Input:**  $\{\tilde{\mathbf{X}}_i^{*,0}, \tilde{\mathbf{U}}_i^{*,0}\}_{i=1}^n$ ,  $\{\frac{d\boldsymbol{\lambda}_i^0}{d\boldsymbol{\theta}}, \frac{d\boldsymbol{\xi}_i^0}{d\boldsymbol{\theta}}\}_{i=1}^n$ ,  $a = 0$ ,  $a_{\text{fp}}$ ,  $\{\{\tau_i^{*,a}, \tilde{\tau}_i^{*,a}\}_{i=1}^n\}_{a=1}^{a_{\text{fp}}}$ ,  $\{\{\boldsymbol{\lambda}_i^{*,a}, \boldsymbol{\xi}_i^{*,a}\}_{i=1}^n\}_{a=1}^{a_{\text{fp}}}$ , and the intermediate results from DDP.

```

1 for  $a < a_{\text{fp}}$  do
2    $\triangleright$  Auxiliary Subproblem 1
3   for  $i \leftarrow 1$  to  $n$  do
4      $\hat{H}_{\tilde{\mathbf{x}}\boldsymbol{\theta},k}^{*,a} \leftarrow$  Solve (35a) with  $\mathbf{X}_i^{*,a}$  and  $\frac{d\boldsymbol{\lambda}_i^a}{d\boldsymbol{\theta}}$ ;
5      $\hat{H}_{\tilde{\mathbf{u}}\boldsymbol{\theta},k}^{*,a} \leftarrow$  Solve (35b) with  $\mathbf{U}_i^{*,a}$  and  $\frac{d\boldsymbol{\xi}_i^a}{d\boldsymbol{\theta}}$ ;
6      $\{\mathbf{X}_i^{*,a}, \mathbf{U}_i^{*,a}\}^{a+1} \leftarrow$  Solve (36) using Lemma 2;
7   end for
8    $\triangleright$  Auxiliary Subproblem 2
9   for  $k \leftarrow 0$  to  $N-1$  do
10     $\hat{L}_{\tilde{\mathbf{x}}\boldsymbol{\theta},k}^{*,a} \leftarrow$  Solve (42a) with  $\mathbf{X}_k^{*,a+1}$  and  $\frac{d\boldsymbol{\lambda}_k^a}{d\boldsymbol{\theta}}$ ;
11     $\hat{L}_{\tilde{\mathbf{u}}\boldsymbol{\theta},k}^{*,a} \leftarrow$  Solve (42b) with  $\mathbf{U}_k^{*,a+1}$  and  $\frac{d\boldsymbol{\xi}_k^a}{d\boldsymbol{\theta}}$ ;
12    Compute  $\hat{L}_{\tilde{\mathbf{x}}\boldsymbol{\theta},k}^{*,a}$ ,  $\hat{L}_{\tilde{\mathbf{x}}\boldsymbol{\theta},k}^{*,a}$ , and  $\hat{L}_{\tilde{\mathbf{u}}\boldsymbol{\theta},k}^{*,a}$ ;
13     $\{\tilde{\mathbf{X}}_k^{*,a}, \tilde{\mathbf{U}}_k^{*,a}\}^{a+1} \leftarrow$  Solve (38) analytically;
14  end for
15   $\hat{L}_{\tilde{\mathbf{x}}\boldsymbol{\theta},N}^{*,a} \leftarrow$  Solve (42a) with  $\mathbf{X}_N^{*,a+1}$  and  $\frac{d\boldsymbol{\lambda}_N^a}{d\boldsymbol{\theta}}$ ;
16  Compute  $\hat{L}_{\tilde{\mathbf{x}}\boldsymbol{\theta},N}^{*,a}$ ;
17   $\tilde{\mathbf{X}}_N^{*,a+1} \leftarrow$  Solve (40) analytically;
18   $\triangleright$  Auxiliary Subproblem 3
19  for  $i \leftarrow 1$  to  $n$  do
20    for  $k \leftarrow 0$  to  $N-1$  do
21       $\{\frac{d\boldsymbol{\lambda}_{i,k}^a}{d\boldsymbol{\theta}}, \frac{d\boldsymbol{\xi}_{i,k}^a}{d\boldsymbol{\theta}}\}^{a+1} \leftarrow$  Solve (43);
22    end for
23     $\frac{d\boldsymbol{\lambda}_{i,N}^{a+1}}{d\boldsymbol{\theta}} \leftarrow$  Solve (43a);
24  end for
25   $a \leftarrow a + 1$ 
26 end for
Output:  $\{\mathbf{X}_i^{*,a}, \mathbf{U}_i^{*,a}\}_{i=1}^n$  and  $\{\tilde{\mathbf{X}}_i^{*,a}, \tilde{\mathbf{U}}_i^{*,a}\}_{i=1}^n$ .

```

---

**Lemma 3.** *The ADMM-LQR-based gradient solver in Algorithm 2 implements the distributed solution for the centralized matrix-valued quadratic programming problem:*

$$\begin{aligned} \min_{\mathbf{X}, \mathbf{U}, \tilde{\mathbf{X}}, \tilde{\mathbf{U}}} \quad & \sum_{i=1}^n \tilde{J}_i(\mathbf{X}_i, \mathbf{U}_i) + \sum_{k=0}^{N-1} \tilde{J}_k(\tilde{\mathbf{X}}_k, \tilde{\mathbf{U}}_k) + \tilde{J}_N(\tilde{\mathbf{X}}_N) \\ \text{s.t.} \quad & \mathbf{X}_{i,k+1} = \mathbf{f}_{\mathbf{x}_{i,k}}^* \mathbf{X}_{i,k} + \mathbf{f}_{\mathbf{u}_{i,k}}^* \mathbf{U}_{i,k} + \mathbf{f}_{\boldsymbol{\theta},k}^*, \\ & \mathbf{X}_{i,0} = \mathbf{0}, \mathbf{X}_{i,k} = \tilde{\mathbf{X}}_{i,k}, \mathbf{U}_{i,k} = \tilde{\mathbf{U}}_{i,k}, \end{aligned} \quad (44)$$

where

$$\begin{aligned} \tilde{J}_i = \sum_{k=0}^{N-1} \text{tr} \left( \frac{1}{2} \begin{bmatrix} \mathbf{X}_{i,k} \\ \mathbf{U}_{i,k} \end{bmatrix}^\top \begin{bmatrix} \mathbf{H}_{\mathbf{x}_i \mathbf{x}_i, k}^{*,a} & \mathbf{H}_{\mathbf{x}_i \mathbf{u}_i, k}^{*,a} \\ \mathbf{H}_{\mathbf{u}_i \mathbf{x}_i, k}^{*,a} & \mathbf{H}_{\mathbf{u}_i \mathbf{u}_i, k}^{*,a} \end{bmatrix} \begin{bmatrix} \mathbf{X}_{i,k} \\ \mathbf{U}_{i,k} \end{bmatrix} \right. \\ \left. + \begin{bmatrix} \nabla_{\boldsymbol{\theta}} \hat{H}_{\mathbf{x}_i, k}^{*,a} \\ \nabla_{\boldsymbol{\theta}} \hat{H}_{\mathbf{u}_i, k}^{*,a} \end{bmatrix}^\top \begin{bmatrix} \mathbf{X}_{i,k} \\ \mathbf{U}_{i,k} \end{bmatrix} \right) \\ + \text{tr} \left( \frac{1}{2} \mathbf{X}_{i,N}^\top \mathbf{H}_{\mathbf{x}_i \mathbf{x}_i, N}^{*,a} \mathbf{X}_{i,N} + \nabla_{\boldsymbol{\theta}} \hat{H}_{\mathbf{x}_i, N}^{*,a} \mathbf{X}_{i,N} \right), \end{aligned} \quad (45)$$

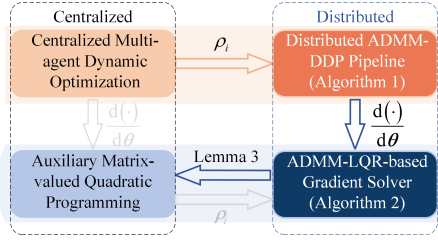


Fig. 3: The relationship between the forward (light gray) and backward (light yellow) passes, and the internal connections between the centralized and distributed formulations within each pass. The light gray arrows indicate disallowed operation paths that are not used in the proposed pipeline.

with  $H_{(\cdot)(\cdot),k}^{*,a} := \frac{\partial^2 \mathcal{H}_{i,k}}{\partial(\cdot)\partial(\cdot)}$  being the Hessians of the Hamiltonian  $\mathcal{H}_{i,k} = \ell_{i,k} + V_{\mathbf{x}_{i,k+1}}^\top \mathbf{f}_i$ ,

$$\begin{aligned} \ddot{\mathbf{J}}_k = \text{tr} \left( \frac{1}{2} \begin{bmatrix} \tilde{\mathbf{X}}_k \\ \tilde{\mathbf{U}}_k \end{bmatrix}^\top \begin{bmatrix} L_{\tilde{\mathbf{x}}\tilde{\mathbf{x}},k}^{*,a}, L_{\tilde{\mathbf{x}}\tilde{\mathbf{u}},k}^{*,a} \\ L_{\tilde{\mathbf{u}}\tilde{\mathbf{x}},k}^{*,a}, L_{\tilde{\mathbf{u}}\tilde{\mathbf{u}},k}^{*,a} \end{bmatrix} \begin{bmatrix} \tilde{\mathbf{X}}_k \\ \tilde{\mathbf{U}}_k \end{bmatrix} \right. \\ \left. + \begin{bmatrix} \nabla_{\theta} \hat{L}_{\tilde{\mathbf{x}},k}^{*,a} \\ \nabla_{\theta} \hat{L}_{\tilde{\mathbf{u}},k}^{*,a} \end{bmatrix}^\top \begin{bmatrix} \tilde{\mathbf{X}}_k \\ \tilde{\mathbf{U}}_k \end{bmatrix} \right), \end{aligned} \quad (46)$$

with  $L_{(\cdot)(\cdot),N}^{*,a} := \frac{\partial^2 \mathcal{L}_k}{\partial(\cdot)\partial(\cdot)}$  being the Hessians of the Lagrangian  $\mathcal{L}_k = -\mu \sum_{i=1}^n [\ln(-\mathbf{g}_{i,k}) + \sum_{j \neq i} \ln(-\mathbf{h}_{ij,k})]$ , and

$$\ddot{\mathbf{J}}_N = \text{tr} \left( \frac{1}{2} \tilde{\mathbf{X}}_N^\top L_{\tilde{\mathbf{x}}\tilde{\mathbf{x}},N}^{*,a} \tilde{\mathbf{X}}_N + \nabla_{\theta} \hat{L}_{\tilde{\mathbf{x}},N}^{*,a} \tilde{\mathbf{X}}_N \right), \quad (47)$$

with  $L_{(\cdot)(\cdot),N}^{*,a} := \frac{\partial^2 \mathcal{L}_N}{\partial(\cdot)\partial(\cdot)}$  being the Hessians of the Lagrangian  $\mathcal{L}_N = -\mu \sum_{i=1}^n [\ln(-\mathbf{g}_{i,N}) + \sum_{j \neq i} \ln(-\mathbf{h}_{ij,N})]$ .

*Proof.* See Appendix-C.  $\square$

The connection between centralized and distributed gradient computation (Lemma 3) is illustrated in Fig. 3, which also shows the forward-backward relationship through the differentiation operator  $\frac{d(\cdot)}{d\theta}$ . Notably, Algorithm 2 cannot be obtained by simply differentiating the centralized formulation of Algorithm 1 and then applying ADMM with the same penalty parameters  $\rho_i$ . In that setting,  $\theta$  excludes  $\rho_i$ , altering terms such as  $\nabla_{\theta} \hat{L}_{\mathbf{x}_i,k}^{*,a}$ ,  $\nabla_{\theta} \hat{L}_{\mathbf{u}_i,k}^{*,a}$ ,  $\nabla_{\theta} \hat{L}_{\tilde{\mathbf{x}},k}^{*,a}$ , and  $\nabla_{\theta} \hat{L}_{\tilde{\mathbf{u}},k}^{*,a}$ .

**Theorem 1.** Assume that: (i) Subproblem 1 is solved using iLQR with the quadratic local cost such as those defined in (20); (ii) the regularization strategy  $\hat{L}_{\tilde{\tau}\tilde{\tau},k}^{*,a} + (\epsilon - \lambda_{\min})\mathbf{I}$  is applied to Auxiliary Subproblem 2, where  $\lambda_{\min}$  is the smallest eigenvalue of  $L_{\tilde{\tau}\tilde{\tau},k}^{*,a}$  and  $\epsilon > 0$  is a constant. Under these assumptions, Problem (44) is convex, the convergence guarantees of ADMM for convex programs apply directly to the proposed gradient solver.

*Proof.* For iLQR, the Hessians of  $\mathcal{H}_{i,k} = \ell_{i,k} + \lambda_{i,k+1}^\top \mathbf{f}_i$  reduce to the Hessians of the cost function  $\ell_{i,k}$ :

$$\begin{bmatrix} H_{\mathbf{x}_i\mathbf{x}_i,k}^{*,a}, H_{\mathbf{x}_i\mathbf{u}_i,k}^{*,a} \\ H_{\mathbf{u}_i\mathbf{x}_i,k}^{*,a}, H_{\mathbf{u}_i\mathbf{u}_i,k}^{*,a} \end{bmatrix} = \begin{bmatrix} \mathbf{Q}_i & \mathbf{0} \\ \mathbf{0} & \mathbf{R}_i \end{bmatrix} \succ \mathbf{0}.$$

With this, (45) becomes convex. Under the 2nd assumption, the smallest eigenvalue of  $L_{\tilde{\tau}\tilde{\tau},k}^{*,a,\text{rg}} = L_{\tilde{\tau}\tilde{\tau},k}^{*,a} + (\epsilon - \lambda_{\min})\mathbf{I}$  is  $\lambda_{\min}(L_{\tilde{\tau}\tilde{\tau},k}^{*,a,\text{rg}}) = \lambda_{\min}(L_{\tilde{\tau}\tilde{\tau},k}^{*,a}) + \epsilon - \lambda_{\min}(L_{\tilde{\tau}\tilde{\tau},k}^{*,a}) > 0$ , making

(46) and (47) convex. Problem (44) minimizes a convex cost subject to affine constraints, and is thus convex.  $\square$

Theorem 1 provides a convergence guarantee for our gradient solver by leveraging classical ADMM theory in convex settings. These assumptions are mild and typically satisfied in practice: quadratic costs and iLQR solvers are standard in robotics, and regularization is routinely used to handle numerical singularities. Although [32] argues that the second-order system derivatives should be included in the gradient computation for full theoretical rigor, our simulations indicate that omitting them does not impair learning performance.

Vanilla ADMM often converges slowly and requires careful parameter tuning. Even with acceleration methods [8], [10] or adaptive penalties [48]–[50], dozens of iterations are typically needed for acceptable accuracy. To accelerate computation, we truncate ADMM to  $a_{\text{tc}}$  iterations ( $a_{\text{tc}} < a_{\text{fp}}$ ) and meta-learn the penalty parameters  $\rho_i$  to achieve rapid residual reduction. Since Algorithm 2 is run with the same number of iterations as the forward pass, this truncation speeds up both the trajectory optimization and the gradient computation. Furthermore, we prove that the resulting gradient errors remain bounded under mild assumptions, as stated in the following theorem.

**Theorem 2.** Define  $\tau_{i,k}^{*,a_{\text{tc}}} := [\mathbf{x}_{i,k}^{*,a_{\text{tc}}}, \mathbf{u}_{i,k}^{*,a_{\text{tc}}}]^\top$  as the optimal solution of agent  $i$  at time step  $k$  of Auxiliary Subsystem 1 under the ADMM truncation and let  $\delta\tau_{i,k} := \|\tau_{i,k}^{*,a_{\text{tc}}} - \tau_{i,k}^{*,a_{\text{fp}}}\|$  denote the corresponding truncation-induced solution error. Assume there exist constants  $L_1, \dots, L_8 > 0$  such that:

$$\begin{aligned} \|\Delta \hat{H}_{\mathbf{x}_i\mathbf{x}_i,k}\| &\leq L_1 \|\delta\tau_{i,k}\|, & \|\Delta \hat{H}_{\mathbf{x}_i\mathbf{u}_i,k}\| &\leq L_2 \|\delta\tau_{i,k}\|, \\ \|\Delta \hat{H}_{\mathbf{u}_i\mathbf{u}_i,k}\| &\leq L_3 \|\delta\tau_{i,k}\|, & \|\Delta \hat{H}_{\mathbf{x}_i\theta,k}\| &\leq L_4 \|\delta\tau_{i,k}\|, \\ \|\Delta \hat{H}_{\mathbf{u}_i\theta,k}\| &\leq L_5 \|\delta\tau_{i,k}\|, & \|\Delta f_{\mathbf{x}_i,k}\| &\leq L_6 \|\delta\tau_{i,k}\|, \\ \|\Delta f_{\mathbf{u}_i,k}\| &\leq L_7 \|\delta\tau_{i,k}\|, & \|\Delta f_{\theta,k}\| &\leq L_8 \|\delta\tau_{i,k}\|. \end{aligned} \quad (48)$$

Then, there exist constants  $L_{X,i,k}, L_{U,i,k} > 0$  such that for all  $k = 0, \dots, N$ , the gradient trajectory deviations satisfy:

$$\|\mathbf{X}_{i,k}^{*,a_{\text{tc}}} - \mathbf{X}_{i,k}^{*,a_{\text{fp}}}\| \leq L_{X,i,k} \sum_{t=0}^{k-1} \|\delta\tau_{i,t}\|, \quad (49a)$$

$$\|\mathbf{U}_{i,k}^{*,a_{\text{tc}}} - \mathbf{U}_{i,k}^{*,a_{\text{fp}}}\| \leq L_{U,i,k} \sum_{t=0}^k \|\delta\tau_{i,t}\|. \quad (49b)$$

*Proof.* See Appendix-D.  $\square$

While the above theorem is motivated by perturbations from ADMM truncation, the same analysis applies to other sources such as solver inaccuracies, model identification errors, and numerical drift. Both our work and Theorem 7 in [33] address matrix perturbations induced by optimal trajectory errors, but their origins differ: [33] focuses solely on solver inaccuracy, whereas our formulation also captures perturbations from ADMM truncation and other algorithmic or modeling errors. This enables a unified treatment of perturbation sources beyond solver inaccuracy. By casting these effects as stage-wise matrix perturbations in the auxiliary matrix-valued LQR subsystem, we derive finite-horizon bounds that characterize how such perturbations propagate through the closed-loop recursions.



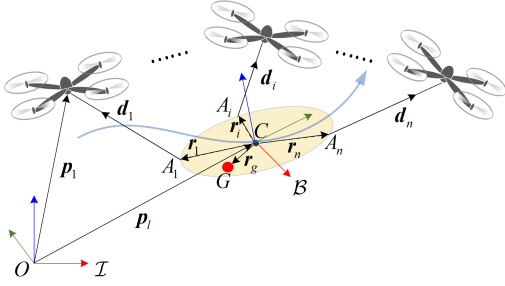


Fig. 4: The multilift system with the definition of coordinate frames. The red point marks the center of mass (CoM) of the load, which is offset from the center of geometry (CoG) by a vector  $\mathbf{r}_g \in \mathbb{R}^3$  in the load body frame  $\mathcal{B}$ .  $A_i$  denotes the cable attachment point of the  $i$ th cable on the load.

## V. APPLICATIONS TO MULTILIFT SYSTEMS

We apply L2C to meta-learn safe and feasible trajectories for a multilift system. Fig. 4 shows the setup:  $n$  quadrotors transport a shared load via  $n$  cables, each linking one quadrotor to the load. The tight inter-agent couplings introduced by the cables necessitate coordination-aware trajectory optimization that goes beyond decoupled or weakly coupled swarm systems.

Let  $m_l \in \mathbb{R}_+$  denote the load's mass,  $\mathbf{J}_l \in \mathbb{R}^{3 \times 3}$  its moment of inertia w.r.t. its CoG,  $\mathbf{p}_l \in \mathbb{R}^3$  the position of the load's CoG in the world frame  $\mathcal{I}$ ,  $\mathbf{v}_l \in \mathbb{R}^3$  its velocity in the body frame  $\mathcal{B}$ ,  $\mathbf{q}_l \in \mathbb{S}^3$  the load's unit quaternion,  $\boldsymbol{\omega}_l \in \mathbb{R}^3$  its angular velocity, and  $\mathbf{F}_l \in \mathbb{R}^3$  and  $\mathbf{M}_l \in \mathbb{R}^3$  the collective cable force and torque on the load's CoG in  $\mathcal{B}$ . We model the load as a 6 DoF rigid-body whose dynamics are given by

$$\dot{\mathbf{p}}_l = \mathbf{R}_l \mathbf{v}_l, \quad (50a)$$

$$\dot{\mathbf{v}}_l = -\dot{\boldsymbol{\omega}}_l^\times \mathbf{r}_g - \boldsymbol{\omega}_l^\times (\mathbf{v}_l + \boldsymbol{\omega}_l^\times \mathbf{r}_g) + \frac{\mathbf{F}_l}{m_l} - \mathbf{R}_l^\top g \mathbf{e}_3, \quad (50b)$$

$$\dot{\mathbf{q}}_l = \frac{1}{2} \boldsymbol{\Omega}(\boldsymbol{\omega}_l) \mathbf{q}_l, \quad (50c)$$

$$\dot{\boldsymbol{\omega}}_l = \mathbf{J}_l^{-1} [\mathbf{M}_l - \mathbf{r}_g^\times \mathbf{R}_l^\top g \mathbf{e}_3 - \boldsymbol{\omega}_l^\times (\mathbf{J}_l \boldsymbol{\omega}_l) + \mathbf{M}_{cp}] \quad (50d)$$

where  $\mathbf{M}_{cp} = -m_l \mathbf{r}_g^\times (\dot{\mathbf{v}}_l + \boldsymbol{\omega}_l^\times \mathbf{v}_l)$ ,  $(\mathbf{a})^\times$  denotes the skew-symmetric matrix form of  $\mathbf{a} \in \mathbb{R}^3$ ,  $\mathbf{R}_l := \mathbf{R}_l(\mathbf{q}_l) \in SO(3)$  is the rotation matrix with  $\mathbf{q}_l$  from  $\mathcal{B}$  to  $\mathcal{I}$ ,  $g$  is the gravitational acceleration,  $\mathbf{e} := [0, 0, 1]^\top$ , and  $\boldsymbol{\Omega}(\boldsymbol{\omega}_l) := \begin{bmatrix} 0 & -\boldsymbol{\omega}_l^\top \\ \boldsymbol{\omega}_l & -\boldsymbol{\omega}_l^\times \end{bmatrix}$ .

Following [53], [56], we formulate the multilift trajectory optimization problem in terms of cable dynamics rather than quadrotor dynamics, thereby improving the numerical efficiency of the formulation. The cable is assumed to be massless as a modeling simplification, and inextensible due to the high stiffness of materials such as Nylon [66]. Let  $\mathbf{d}_i \in \mathbb{S}^2$  denote the unit direction vector of the  $i$ th cable in  $\mathcal{I}$ , pointing from  $A_i$  to the  $i$ th quadrotor. Let  $\boldsymbol{\omega}_i \in \mathbb{R}^3$  and  $\boldsymbol{\gamma}_i \in \mathbb{R}^3$  represent its angular velocity and angular acceleration, respectively;  $t_i \in \mathbb{R}$  its tension magnitude;  $\dot{v}_i \in \mathbb{R}$  the rate of change of tension; and  $a_i \in \mathbb{R}$  the acceleration of tension change. When the  $i$ th cable is taut, its dynamics are described by

$$\dot{\mathbf{d}}_i = \boldsymbol{\omega}_i^\times \mathbf{d}_i, \quad \dot{\boldsymbol{\omega}}_i = \boldsymbol{\gamma}_i, \quad \dot{t}_i = v_i, \quad \dot{v}_i = a_i. \quad (51)$$

The validity of the dynamics (51) requires that all the cables remain taut. Maintaining tautness also ensures that the load

stays under control during cooperative flight. This requirement is enforced through the following cable tension constraint:

$$0 < t_i \leq t_{\max}, \quad \forall i \in \{1, \dots, n\}, \quad (52)$$

where  $t_{\max} \in \mathbb{R}_+$  is the maximum allowable tension force.

The taut cables impose additional kinodynamic constraints on the system. First, the kinematics of each quadrotor and the load are coupled through the length constraint

$$\mathbf{p}_i = \mathbf{p}_l + \mathbf{R}_l \mathbf{r}_i + l_i \mathbf{d}_i, \quad \forall i \in \{1, \dots, n\}, \quad (53)$$

where  $\mathbf{p}_i \in \mathbb{R}^3$  is the position of the  $i$ th quadrotor's CoM in  $\mathcal{I}$ ,  $\mathbf{r}_i \in \mathbb{R}^3$  is the coordinate of  $A_i$  in  $\mathcal{B}$ , and  $l_i \in \mathbb{R}_+$  is the length of the  $i$ th cable. To guarantee safety, we require that the quadrotors avoid collisions with each other and with obstacles. The corresponding kinematic constraints are

$$\|\mathbf{p}_i - \mathbf{p}_j\| \geq d_{\min}^q, \quad \forall i, j \in \{1, \dots, n\}, \quad i \neq j, \quad (54a)$$

$$\|\mathbf{p}_i - \mathbf{p}_o\| \geq d_{\min}^o, \quad \forall i \in \{1, \dots, n\}, \quad (54b)$$

where  $d_{\min}^q \in \mathbb{R}_+$  is the minimum separation between any two quadrotors,  $\mathbf{p}_o \in \mathbb{R}^3$  is the position of the obstacle's CoG in  $\mathcal{I}$ , and  $d_{\min}^o$  is the minimum distance between each quadrotor's CoM and the obstacle's CoG. In addition to the above kinematic constraints, the load and cable dynamics in (50) and (51) are coupled through the following cable-driven force and torque constraints:

$$\begin{bmatrix} \mathbf{F}_l \\ \mathbf{M}_l \end{bmatrix} = \underbrace{\begin{bmatrix} \mathbf{I} & \dots & \mathbf{I} \\ \mathbf{r}_1^\times & \dots & \mathbf{r}_n^\times \end{bmatrix}}_{:=\mathbf{P}} \begin{bmatrix} \mathbf{R}_l^\top t_1 \mathbf{d}_1 \\ \vdots \\ \mathbf{R}_l^\top t_n \mathbf{d}_n \end{bmatrix}. \quad (55)$$

Although the quadrotor dynamics are not explicitly included in the system model, they are accounted for through the following thrust constraint, which prevents overloading:

$$\|m_i (\ddot{\mathbf{p}}_i + g \mathbf{e}_3) + t_i \mathbf{d}_i\| \leq f_{\max}, \quad \forall i \in \{1, \dots, n\}, \quad (56)$$

where  $m_i \in \mathbb{R}_+$  is the  $i$ th quadrotor's mass,  $f_{\max} \in \mathbb{R}_+$  is the maximum collective thrust generated by its four motors, and  $\ddot{\mathbf{p}}_i \in \mathbb{R}^3$  is the acceleration of the quadrotor's CoM.

Let  $\mathbf{x}_{l,k} = [\mathbf{p}_{l,k}; \mathbf{v}_{l,k}; \mathbf{q}_{l,k}; \boldsymbol{\omega}_{l,k}]$  and  $\mathbf{u}_{l,k} = [\mathbf{F}_{l,k}; \mathbf{M}_{l,k}]$  denote the load's state and control at time step  $k$ . Similarly, let  $\mathbf{x}_{i,k} = [\mathbf{d}_{i,k}; \boldsymbol{\omega}_{i,k}; t_{i,k}; v_{i,k}]$  and  $\mathbf{u}_{i,k} = [\boldsymbol{\gamma}_{i,k}; a_{i,k}]$  denote the  $i$ th cable's state and control at  $k$ . We adopt the following quadratic costs for the load and each cable, as commonly used in multilift trajectory optimization [53], [56], [59]:

$$J_l = \sum_{k=0}^{N-1} \frac{1}{2} \left( \|\mathbf{x}_{l,k} - \mathbf{x}_{l,k}^{\text{ref}}\|_{\mathbf{Q}}^2 + \|\mathbf{u}_{l,k} - \mathbf{u}_{l,k}^{\text{ref}}\|_{\mathbf{R}}^2 \right) + \frac{1}{2} \|\mathbf{x}_{l,N} - \mathbf{x}_{l,N}^{\text{ref}}\|_{\mathbf{Q}_N}^2, \quad (57a)$$

$$J_i = \sum_{k=0}^{N-1} \frac{1}{2} \left( \|\mathbf{x}_{i,k} - \mathbf{x}_{i,k}^{\text{ref}}\|_{\mathbf{Q}_i}^2 + \|\mathbf{u}_{i,k} - \mathbf{u}_{i,k}^{\text{ref}}\|_{\mathbf{R}_i}^2 \right) + \frac{1}{2} \|\mathbf{x}_{i,N} - \mathbf{x}_{i,N}^{\text{ref}}\|_{\mathbf{Q}_{i,N}}^2. \quad (57b)$$



The multilift trajectory planning problem can therefore be cast as the following centralized optimization problem:

$$\min_{\mathbf{x}_l, \mathbf{u}_l, \{\mathbf{x}_i, \mathbf{u}_i\}_{i=1}^n} J_l(\mathbf{x}_l, \mathbf{u}_l) + \sum_{i=1}^n J_i(\mathbf{x}_i, \mathbf{u}_i) \quad (58a)$$

$$\text{s.t. } \mathbf{x}_{l,k+1} = \mathbf{f}_l(\mathbf{x}_{l,k}, \mathbf{u}_{l,k}), \mathbf{x}_{l,0} : \text{given}, \quad (58b)$$

$$\mathbf{x}_{i,k+1} = \mathbf{f}_i(\mathbf{x}_{i,k}, \mathbf{u}_{i,k}), \mathbf{x}_{i,0} : \text{given}, \quad (58c)$$

$$0 < t_{i,k} \leq t_{\max}, \quad (58d)$$

$$\text{inter-agent kinodynamic constraints:} \quad (58e) \\ (54), (55), (56),$$

where  $\mathbf{f}_l$  and  $\mathbf{f}_i$  are the discrete-time dynamics corresponding to (50) and (51), respectively. We solve Problem (58) using Algorithm 1 by applying the safe-copy-variable strategy:

$$\mathbf{x}_{l,k} = \tilde{\mathbf{x}}_{l,k}, \mathbf{u}_{l,k} = \tilde{\mathbf{u}}_{l,k}, \mathbf{x}_{i,k} = \tilde{\mathbf{x}}_{i,k}, \mathbf{u}_{i,k} = \tilde{\mathbf{u}}_{i,k}. \quad (59)$$

For the distributed solution of Problem (58), the meta-learned key hyperparameters include the weights in the local cost functions (57a) and (57b), along with the ADMM penalty parameters  $\rho_l$  for the load and  $\rho_i$  for each cable. Since all cables share the same dynamics (51) and are isomorphic, they use a common set of weights and a shared  $\rho_c$  to improve scalability. Let  $\theta_l = [\text{vec}(\mathbf{Q}), \text{vec}(\mathbf{R}), \text{vec}(\mathbf{Q}_N), \rho_l]$  denote the load's hyperparameters, and  $\theta_c = [\text{vec}(\mathbf{Q}_c), \text{vec}(\mathbf{R}_c), \text{vec}(\mathbf{Q}_{c,N}), \rho_c]$  denote those shared by all cables. These are modeled using two lightweight neural networks to enable task adaptation, and the full hyperparameter set is denoted by  $\theta = [\theta_l, \theta_c]$ .

Following the formulation in subsection III-C, we define the upper-level loss for  $M$  multilift tasks as:

$$L = \frac{1}{M} \sum_{t=1}^M \underbrace{\left( \ell_{l,p} + \ell_{l,r} + \sum_{i=1}^n (\ell_{i,p} + \ell_{i,r}) \right)}_{:=L_t}, \quad (60)$$

where  $\ell_{l,p} = \|\boldsymbol{\tau}_l - \boldsymbol{\tau}_l^{\text{ref}}\|_{\mathbf{W}}^2$  is the tracking error between the optimized trajectory and the reference waypoints, with  $\mathbf{W}$  being the weighting matrix,  $\ell_{l,r} = \|\boldsymbol{\tau}_l - \tilde{\boldsymbol{\tau}}_l\|_2^2$  is the ADMM residual for the load, and the same definitions apply to  $\ell_{i,p}$  and  $\ell_{i,r}$  for all the cables.

Including references in the cost (57) facilitates solving multilift trajectory optimization problems like (58), as shown in [59], by guiding the solution and avoiding deadlock. The load waypoints  $\mathbf{x}_l^{\text{ref}}$  can be generated via standard single-agent path planners, and the controls  $\mathbf{u}_l^{\text{ref}}$  can be estimated using the load dynamics. In contrast, generating feasible cable waypoints  $\mathbf{x}_i^{\text{ref}}$  is more difficult due to the dynamic constraints (55). Rather than directly meta-learning  $\mathbf{x}_i^{\text{ref}}$  as part of  $\theta_c$ , which cannot guarantee feasibility, we meta-learn the cost weights of the following optimization problem to generate them:

$$\min_{\mathbf{x}_l, \mathbf{u}_l, \Pi} J_l(\mathbf{x}_l, \mathbf{u}_l) + \sum_{k=0}^{N-1} \sum_{i=1}^n \frac{1}{2} \|\mathbf{t}_{i,k} - \mathbf{t}^{\text{ref}}\|_{\mathbf{R}_t}^2 \quad (61a)$$

$$\text{s.t. } \mathbf{x}_{l,k+1} = \mathbf{f}_l(\mathbf{x}_{l,k}, \mathbf{u}_{l,k}), \mathbf{x}_{l,0} : \text{given}, \quad (61b)$$

$$\mathbf{t}_k = \mathbf{P}^\dagger \mathbf{u}_{l,k} + \mathbf{N} \Pi_k, \quad (61c)$$

$$0 < \|\mathbf{t}_{i,k}\| \leq t_{\max}, \quad (61d)$$

$$\text{kinematic constraints: (54),} \quad (61e)$$

where  $J_l$  is the same as defined in (57a),  $\mathbf{t}^{\text{ref}} = [0; 0; \frac{m_l g}{n}]^\top$  is the uniform load gravity allocation per cable,  $\mathbf{P}^\dagger$  is the pseudo-inverse of  $\mathbf{P}$ ,  $\mathbf{N} \in \mathbb{R}^{3n \times (3n-6)}$  is the basis of the null space of  $\mathbf{P}$ ,  $\Pi_k \in \mathbb{R}^{3n-6}$  spans the null space,  $\mathbf{t}_{i,k}$  is the  $i$ th cable's tension in  $\mathcal{B}$ , extracted from  $\mathbf{t}_k$ , and  $\mathbf{p}_i$  in (61e) is given by  $\mathbf{p}_{i,k} = \mathbf{p}_{l,k} + \mathbf{R}_{l,k}(\mathbf{r}_i + l_i \frac{\mathbf{t}_{i,k}}{\|\mathbf{t}_{i,k}\|})$ .

Since the cable dynamics are omitted, (61) reduces to a single-agent problem. To improve computational efficiency, it can still be solved using Algorithm 1 by setting  $n = 1$  and applying the safe-copy-variable strategy (59). In this case, we define the meta-learned hyperparameters as the weights in (61a) and the associated ADMM penalty parameter  $\rho_{ls}$ , collectively denoted as  $\theta_{ls} = [\text{vec}(\mathbf{Q}), \text{vec}(\mathbf{R}), \text{vec}(\mathbf{Q}_N), \text{vec}(\mathbf{R}_t), \rho_{ls}]$ , and modeled using a neural network. The feasible cable references are given by  $\mathbf{x}_{i,k}^{\text{ref}} = [\frac{\mathbf{t}_{i,k}^*}{\|\mathbf{t}_{i,k}^*\|}; 0; \|\mathbf{t}_{i,k}^*\|; 0]$  and  $\mathbf{u}_{i,k}^{\text{ref}} = \mathbf{0}$ , where  $\omega_{i,k}^{\text{ref}}$ ,  $v_{i,k}^{\text{ref}}$ , and  $\mathbf{u}_{i,k}^{\text{ref}}$  are approximated as zero since they are not optimized in Problem (61) and thus cannot be recovered. These approximations, together with the estimation of  $\mathbf{u}_{l,k}^{\text{ref}}$ , require careful tuning of the associated cost weights, which is handled by the proposed meta-learning framework.

By reducing (60) to the single-agent case, the upper-level loss for Problem (61) becomes:

$$L_{ls} = \frac{1}{M} \sum_{t=1}^M \underbrace{(\ell_{l,p} + \ell_{l,r})}_{:=L_{ls,t}}. \quad (62)$$

In training, we first meta-learn  $\theta_{ls}$  to generate feasible cable references. We then meta-learn  $\theta_l$  and  $\theta_c$  to generate dynamically feasible cable trajectories. The complete training procedure is summarized in Algorithm 3.

In practice, we adopt an efficient sparse parameterization for the hyperparameters. All the cost weights are set as diagonal matrices to reduce the problem's size. The diagonal entries of  $\mathbf{Q}$ ,  $\mathbf{R}$ , and  $\mathbf{Q}_N$  are parameterized as  $Q_{\cdot} = w_{\min} + (w_{\max} - w_{\min})q_{\cdot}$ ,  $R_{\cdot} = w_{\min} + (w_{\max} - w_{\min})r_{\cdot}$ , and  $Q_{N,\cdot} = w_{\min} + (w_{\max} - w_{\min})q_{N,\cdot}$ , where  $w_{\min}, w_{\max} \in \mathbb{R}+$  define the parameter bounds and the subscript “ $\cdot$ ” denotes the index. The ADMM penalty parameter is similarly parameterized as  $\rho_l = w_{\min} + (w_{\max} - w_{\min})\bar{\rho}_l$ . Under this scheme, the neural network output for the load becomes  $\Theta_l = [q_{\cdot}, q_{N,\cdot}, r_{\cdot}, \bar{\rho}_l] \in \mathbb{R}^{33}$  where “ $\cdot$ ” denotes the dimension of a vector collecting the diagonal elements like  $p_{\cdot} = [p_1, \dots]$ . This parameterization strategy applies similarly to the cable and to Problem (61), yielding the network outputs  $\Theta_c \in \mathbb{R}^{21}$  and  $\Theta_{ls} \in \mathbb{R}^{36}$ , respectively. To reflect this parameterization, the chain rule in the gradient computation (23) must additionally account for the gradients  $\frac{\partial \theta_l}{\partial \Theta_l}$ ,  $\frac{\partial \theta_c}{\partial \Theta_c}$ , and  $\frac{\partial \theta_{ls}}{\partial \Theta_{ls}}$ .

## VI. EXPERIMENTS

We validate the effectiveness of L2C on multilift systems through high-fidelity simulations. Fig. 5 illustrates the experimental setup, where multiple quadrotors transport a load along a reference trajectory while avoiding collisions with obstacles and each other. L2C is applied to meta-learn collision-free, dynamically feasible trajectories across tasks. In each task, the load's CoM is randomly offset from its CoG in the body frame, reflecting the practical difficulty of achieving uniform

**Algorithm 3: Multilift L2C Framework**


---

**Input:**  $\tau_l^{\text{ref}}, \varpi_l^0, \varpi_c^0, \varpi_{ls}^0$ .

1  $\triangleright$  Meta-learn cable references

2 **while**  $L_{ls}$  not converged **do**

3   **for**  $t \leftarrow 1$  to  $M$  **do**

4     **Forward Pass:**

5     Compute the adaptive hyperparameters  $\theta_{ls,t}$  using  $\theta_{ls,t} = \pi_{ls}(\chi_t)$  with  $\varpi_{ls}$ ;

6     Solve Problem (61) using Algorithm 1 to obtain  $\tau_l^*, \tilde{\tau}_l^*$ , and  $\Pi^*$ ;

7     Compute the task loss  $L_{ls,t}$  using (62);

8     **Backward Pass:**

9     Compute  $\frac{d\tau_l^*}{d\theta_{ls}}$  and  $\frac{d\tilde{\tau}_l^*}{d\theta_{ls}}$  using Algorithm 2;

10    Compute  $\frac{dL_{ls,t}}{d\varpi_{ls}}$  using (23) ( $M = 1$  and  $n = 1$ )

11   **end for**

12   Compute  $L_{ls} = \frac{1}{M} \sum_{t=1}^M L_{ls,t}$ ;

13   Compute  $\frac{dL_{ls}}{d\varpi_{ls}} = \frac{1}{M} \sum_{t=1}^M \frac{dL_{ls,t}}{d\varpi_{ls}}$ ;

14   Update  $\varpi_{ls}$  using gradient-based optimization;

15    $\triangleright$  one training episode

15 **end while**

16  $\triangleright$  Meta-learn cable trajectories

17 **while**  $L$  not converged **do**

18   **for**  $t \leftarrow 1$  to  $M$  **do**

19     **Forward Pass:**

20     Compute the adaptive hyperparameters  $\theta_{ls,t}$  using  $\theta_{ls,t} = \pi_{ls}(\chi_t)$  with  $\varpi_{ls}^*$ ;

21     Solve Problem (61) using Algorithm 1 to obtain  $\tau_l^*, \tilde{\tau}_l^*$ , and  $\Pi^*$ ;

22     Compute  $x_i^{\text{ref}}$  and  $u_i^{\text{ref}}$  using  $\tilde{\tau}_l^*$  and  $\Pi^*$ ;

23     Compute the load adaptive hyperparameters  $\theta_{l,t}$  using  $\theta_{l,t} = \pi_l(\chi_t)$  with  $\varpi_l$ ;

24     Compute the cable adaptive hyperparameters  $\theta_{c,t}$  using  $\theta_{c,t} = \pi_c(\chi_t)$  with  $\varpi_c$ ;

25     Solve Problem (58) using Algorithm 1 to obtain  $\tau_l^*, \tilde{\tau}_l^*, \{\tau_i^*\}_{i=1}^n$ , and  $\{\tilde{\tau}_i^*\}_{i=1}^n$ ;

26     Compute the task loss  $L_t$  using (60);

27     **Backward Pass:**

28     Compute  $\frac{d\tau_l^*}{d\theta}, \{\frac{d\tilde{\tau}_l^*}{d\theta}\}_{i=1}^n, \{\frac{d\tau_i^*}{d\theta}\}_{i=1}^n$  and  $\{\frac{d\tilde{\tau}_i^*}{d\theta}\}_{i=1}^n$  using Algorithm 2;

29     Compute  $\frac{dL_t}{d\varpi_l}$  and  $\frac{dL_t}{d\varpi_c}$  using (23) ( $M = 1$ );

30   **end for**

31   Compute  $L = \frac{1}{M} \sum_{t=1}^M L_t$ ;

32   Compute  $\frac{dL}{d\varpi_l} = \frac{1}{M} \sum_{t=1}^M \frac{dL_t}{d\varpi_l}$ ;

33   Compute  $\frac{dL}{d\varpi_c} = \frac{1}{M} \sum_{t=1}^M \frac{dL_t}{d\varpi_c}$ ;

34   Update  $\varpi_l$  and  $\varpi_c$  using gradient-based optimization;  $\triangleright$  one training episode

35 **end while**

**Output:**  $\varpi_{ls}^*, \varpi_l^*$ , and  $\varpi_c^*$ .

---

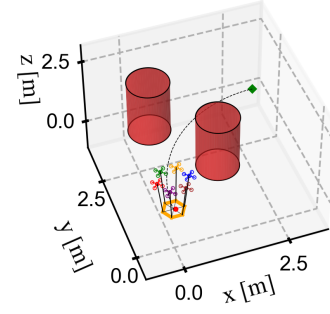


Fig. 5: Multilift experimental scenario. Two red cylinders denote obstacles, the red point on the load marks its CoM (offset from the CoG), and the green point marks the target position.

mass distribution. Specifically, we demonstrate the following advantages of L2C:

- 1) High efficiency in gradient computation compared with state-of-the-art methods (Section VI-A);
- 2) Effective learning of adaptive hyperparameters that enable the ADMM-DDP pipeline to generate dynamically feasible trajectories across tasks, yielding system formations adaptive to different load CoM offsets when passing obstacles (Section VI-B);
- 3) Strong scalability with different quadrotor counts in new settings without additional tuning (Section VI-C).

In our experiments, we design three multilayer perceptron (MLP) networks to generate task-adaptive  $\Theta_{ls}$ ,  $\Theta_l$ , and  $\Theta_c$ . Each network has two hidden layers with the rectified linear unit (ReLU) activation  $\phi(x) = \max(x, 0)$ . To match the sparse parameterization (Section V), the output layers use the sigmoid activation  $S(x) = (1 + \exp(-x))^{-1}$ . The corresponding parameter bounds are set to  $w_{\min} = 0.01$  and  $w_{\max} = 1000$ . The MLP for  $\Theta_{ls}$  takes as input  $\|\mathbf{r}_g\|$ , the magnitude of the load's CoM offset vector, while the MLPs for  $\Theta_l$  and  $\Theta_c$  take the planar coordinates  $[x; y]$  of  $\mathbf{r}_g$ . The three MLPs have architectures  $1 \rightarrow 16 \rightarrow 32 \rightarrow 36$ ,  $2 \rightarrow 16 \rightarrow 32 \rightarrow 33$ , and  $2 \rightarrow 10 \rightarrow 20 \rightarrow 21$ , resulting in 1764, 1681, and 691 network parameters, respectively, lightweight compared with typical deep neural networks. Training is conducted across  $M = 10$  tasks, where in each task the planar coordinates of  $\mathbf{r}_g$  are randomized as  $[\|\mathbf{r}_g\| \cos \alpha; \|\mathbf{r}_g\| \sin \alpha]$  with  $\|\mathbf{r}_g\| \sim \mathcal{U}(0, 0.04 \text{ m})$  and  $\alpha \sim \mathcal{U}(0, 2\pi \text{ rad})$ .

We implement L2C in Python, solving Subproblem 1 (the dynamic optimization (7)) using iLQR and Subproblem 2 (the stage-wise static optimizations (9) and (10)) with ipopt via CasADi [67]. The ADMM iteration counts in Algorithms 1 and 2 are truncated to  $a_{tc} = 2$  for accelerating the meta-trajectory optimization. These MLPs are built using PyTorch [30] and trained with Adam [68]. To align with PyTorch's training procedure, we customize the upper-level losses (60) and (62). For example, the customized loss for training the neural adaptive  $\Theta_{ls}$  is defined by  $L_{\text{py},ls} = \frac{1}{M} \sum_{t=1}^M \frac{dL_{ls,t}}{d\Theta_{ls,t}} \Theta_{ls,t}$ , where  $\frac{dL_{ls,t}}{d\Theta_{ls,t}} = \left( \frac{\partial L_{ls,t}}{\partial \tau_{l,t}^*} \frac{d\tau_{l,t}^*}{d\theta_{ls,t}} + \frac{\partial L_{ls,t}}{\partial \tilde{\tau}_{l,t}^*} \frac{d\tilde{\tau}_{l,t}^*}{d\theta_{ls,t}} \right) \frac{\partial \theta_{ls,t}}{\partial \Theta_{ls,t}}$  denotes the gradient of the task loss  $L_{ls,t}$  w.r.t.  $\Theta_{ls,t}$  evaluated at the current parameters. This ensures that  $\frac{dL_{\text{py},ls}}{d\varpi_{ls}} = \frac{dL_{ls}}{d\varpi_{ls}}$ .

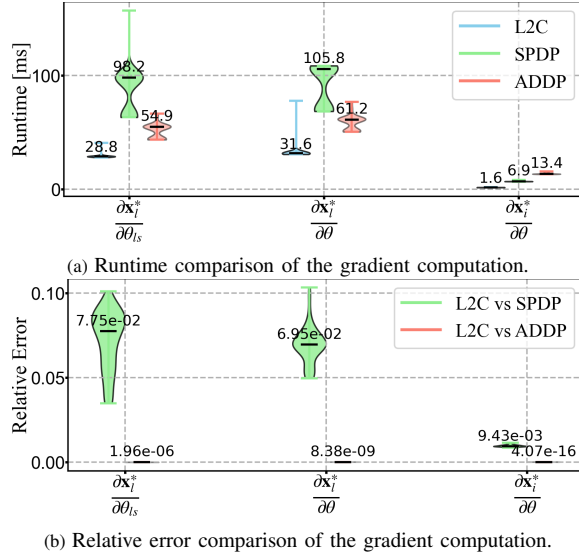


Fig. 6: Boxplots over 100 runs comparing runtime and relative errors of the gradient computation for dynamic optimization (7). The relative errors are measured between L2C and SPDP, and between L2C and ADDP, defined respectively as  $\frac{1}{N} \sum_{k=1}^N \frac{\|\mathbf{x}_{l,k}^{L2C} - \mathbf{x}_{l,k}^{SPDP}\|_F}{\|\mathbf{x}_{l,k}^{L2C}\|_F}$  and  $\frac{1}{N} \sum_{k=1}^N \frac{\|\mathbf{x}_{l,k}^{L2C} - \mathbf{x}_{l,k}^{ADDP}\|_F}{\|\mathbf{x}_{l,k}^{L2C}\|_F}$ , where  $\mathbf{x}_{l,k}^{L2C}$  is the gradient  $\mathbf{x}_{l,k}^*$  w.r.t.  $\theta_{ls}$  or  $\theta$ , obtained by L2C. The data shown in the plots denote the median values. The runtime is measured in a workstation with a 11th Gen Intel Core i7-11700K processor.

### A. Efficient Gradient Computation

Before showing the trajectory optimization performance of L2C, we first test its computational efficiency in training by measuring the CPU runtime of Lemma 2 and comparing it with two state-of-the-art gradient computation methods: safe PDP (SPDP) [36] and augmented DDP (ADDP) [38]. For fair comparisons, Subproblem 1 in the ADMM-DDP pipeline is solved using iLQR across all three methods. The Hamiltonian Hessians, such as  $H_{xx,k}^*$ ,  $H_{xu,k}^*$ , and  $H_{uu,k}^*$ , are computed from iLQR and reused by all three methods for the gradient computation, thus are excluded from the CPU runtime. This enables us to compare runtime differences arising solely from their algorithmic structures. To obtain the gradients of Problem (7), SPDP solves the auxiliary matrix-valued LQR problem (31) via PMP conditions (Lemma 5.2 in [35]), yielding recursions structurally different from those in the DDP solver. ADDP augments the state of Problem (7) with  $\theta$  and performs the gradient computation by running a single DDP iteration on the augmented state  $\mathbf{y} := [\mathbf{x}; \theta]$  (Theorem III.3 in [38]). Unlike L2C, this requires Riccati recursions over larger matrices such as  $V_{yy}$ , and iterates redundant terms  $V_{\theta\theta}$  (see Appendix-B).

Fig. 6a compares the CPU runtime of the three methods on a long-horizon planning task with  $N = 100$ , evaluated for three gradient trajectories  $\frac{\partial \mathbf{x}_{l,k}^*}{\partial \theta_{ls}} \in \mathbb{R}^{13 \times 36}$  (Subproblem 1 for the distributed solution of Problem (61)),  $\frac{\partial \mathbf{x}_{l,k}^*}{\partial \theta} \in \mathbb{R}^{13 \times 54}$ , and  $\frac{\partial \mathbf{x}_{l,k}^*}{\partial \theta} \in \mathbb{R}^{8 \times 54}$  (Subproblem 1 for the distributed solution of Problem (58)). The runtime of each method scales with the matrix dimension of the gradient. L2C outperforms the others in all the three gradient trajectories, achieving up to 88% faster computation. Compared to SPDP, this advantage stems from the efficient reuse of key DDP results in the forward

pass, such as Riccati recursions and feedback gains, due to the structural similarity between the DDP solver and the Bellman's principle-based recursive solutions of the matrix-valued LQR problem. Compared to ADDP, L2C further benefits from the more compact form of the recursions, avoiding iterations over the redundant terms. Our approach is theoretically equivalent to both SPDP and ADDP (Appendix-A and B) in computing the gradients for dynamic optimization. To validate this, we compute relative gradient errors between L2C and these state-of-the-art methods (see definition below Fig. 6). As shown in Fig. 6b, the maximum error across all the gradient trajectories is below 10%, confirming the theoretical equivalence.

### B. Effective Meta-Learning

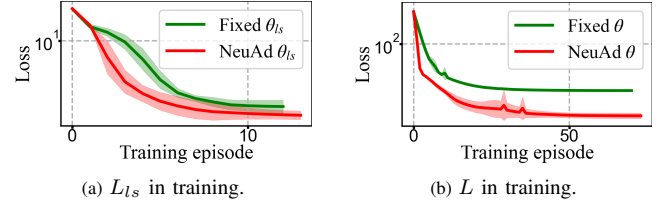


Fig. 7: Upper-level loss comparisons for meta-learning the distributed solutions of Problem (61) and Problem (58). NeuAd denotes neural adaptive. For both neural adaptive and fixed hyperparameters, Algorithm 3 is run five times, with randomly initialized networks for the neural adaptive case and randomly initialized hyperparameters for the fixed case. The solid line shows the mean, and the shaded region indicates the standard deviation.

To show the second advantage of our method, we apply L2C to meta-learn collision-free, dynamically feasible trajectories for a six-quadrotor multilift system in a tightly confined space (Fig. 5). We first conduct ablation studies, comparing L2C with neural adaptive hyperparameters against L2C with fixed ones to highlight the benefits of adaptivity. The fixed version is trained using Algorithm 2, without modeling the hyperparameters via neural networks. Fig. 7 compares the training losses of both versions under the same conditions in two scenarios: (a) meta-learning cable references (Fig. 7a) and (b) meta-learning cable trajectories (Fig. 7b). Although both versions exhibit efficient training convergence within merely tens of episodes, the loss of the adaptive version stabilizes at a much smaller value, indicating better trajectory optimization performance.

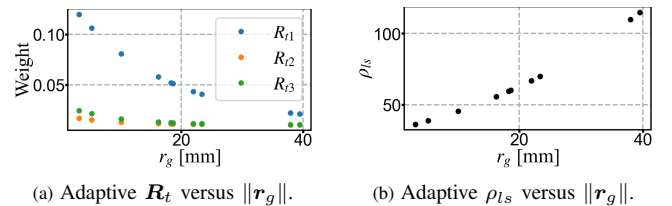


Fig. 8: Meta-learned hyperparameters adaptive to varying magnitudes of the load's CoM vector  $r_g := \|r_g\|$  across 10 tasks.

To demonstrate the adaptivity, Fig. 8 plots the meta-learned hyperparameters against varying load CoM vector magnitudes, randomly generated across ten tasks. These parameters appear in the stage-wise cost of Subproblem 2 under scenario (a):

$$J_{2ls,k} = \sum_{i=1}^n \frac{1}{2} \|\mathbf{t}_{i,k} - \mathbf{t}^{\text{ref}}\|_{\mathbf{R}_t}^2 + \frac{\rho_{ls}}{2} \text{ADMM-Residuals}.$$

The weight  $\mathbf{R}_t$  and the ADMM penalty parameter  $\rho_{ls}$  control the distribution of the cable tension forces and the enforcement of the consensus between the safe-copied and the original variables. As defined below (61),  $\mathbf{t}^{\text{ref}}$  is the reference tension, representing the average load gravity per cable. When  $r_g = 0$ , a large  $\mathbf{R}_t$  and a small  $\rho_{ls}$  drive the tensions toward  $\mathbf{t}^{\text{ref}}$ , yielding uniform load sharing. As  $r_g$  increases, a smaller  $\mathbf{R}_t$  and a larger  $\rho_{ls}$  enable non-uniform sharing to balance the load's attitude. This changing pattern, visible in Figs. 8a and 8b, confirms that the meta-learned hyperparameters adapt effectively to  $r_g$ . Figs. 9a and 9b exemplify the adaptivity of the cable tension distributions to different  $r_g$  values. As can be seen, a large  $r_g$  leads to significant differences among the cable tensions, whereas an extremely small  $r_g$  greatly reduces these differences, aligning with the expected behavior.

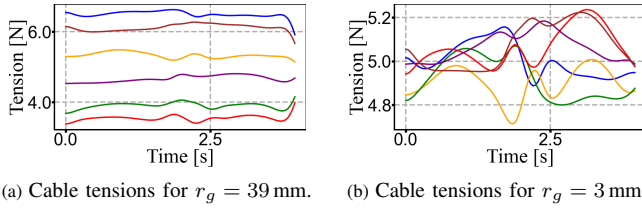


Fig. 9: Comparison of the cable tensions during flight for different  $r_g$  values. The load mass used in training is 3 kg.

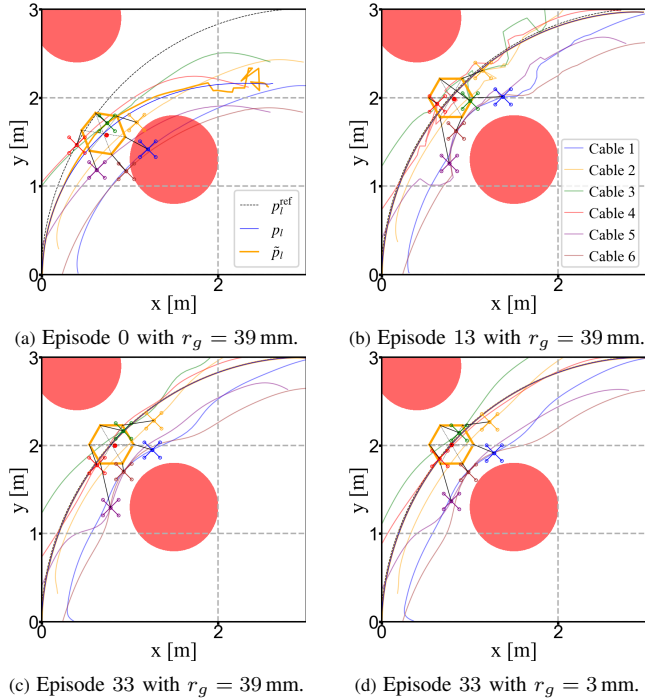


Fig. 10: Comparisons of the cable trajectories and the quadrotor formation shapes with different  $r_g$  values. Figs. 10a and 10b show the training process of the multilift system with  $r_g = 39$  mm in meta-learning  $\theta_{ls}$  for generating the cable references. Figs. 10c and 10d show two groups of the dynamically-feasible cable trajectories for  $r_g = 39$  mm and  $r_g = 3$  mm, respectively, at the last episode of meta-learning  $\theta$ .

Figs. 10a and 10b compare the cable references in a task with  $r_g = 39$  mm at two training episodes in meta-learning  $\theta_{ls}$ . At episode 0, the initial  $\theta_{ls}$  leads to the cable references colliding with the obstacle and to large violations of the

ADMM consensus constraints between the load's original ( $p_i$ ) and safe-copied ( $\tilde{p}_i$ ) trajectories. By episode 13, both the collisions and the violations are minimized, indicating the effective joint learning of the DDP weights and the ADMM penalty parameter. The trained cable references satisfy the cable-driven dynamic constraints (55), enabling the load to accurately track its reference trajectory generated by a standard single-agent planner such as the minimum snap method [69]. However, these cable references exhibit zig-zag discontinuities, as exemplified in Cables 3 and 5 in Fig. 10b. Such discontinuities pose challenges for lower-level feedback controllers to track in practice. By accounting for the cable dynamics (51), we meta-learn adaptive  $\theta$  for the distributed solution of Problem (58) to generate smooth, dynamically feasible cable trajectories that closely track their references while satisfying the inter-agent kinodynamic constraints, as shown in Fig. 10c for the same  $r_g$  as in Fig. 10b. When  $r_g$  is reduced to 3 mm, Fig. 10d illustrates a distinct formation shape during the obstacle traversal, clearly confirming that the trained cable trajectories effectively adapt to  $r_g$ .

### C. Scalability With Quadrotor Counts

To demonstrate the third advantage of our approach, we evaluate the closed-loop dynamic feasibility of the trained cable trajectories across different team sizes in a high-fidelity software-in-the-loop (SITL) simulation. This environment is built with IsaacSIM [60], using the off-the-shelf PX4 software as the quadrotor feedback controller. In addition to the six-quadrotor team used in training, we test two additional team sizes: three and seven quadrotors. For each team, the cable trajectories are generated offline by first solving Problem (61) using Algorithm 1 ( $n = 1$ ) with the trained  $\theta_{ls}$ , followed by solving Problem (58) using Algorithm 1 with the trained  $\theta$ , without additional tuning. To demonstrate generalizability to new load dynamics unseen during training, we specify a new load CoM vector  $\mathbf{r}_g$ , whose magnitude  $r_g$  and planar coordinates are used as inputs to the MLPs for generating the adaptive  $\theta_{ls}$  and  $\theta$ . We also update the load reference trajectory with a new velocity profile and relocate the enlarged obstacles to form a new flight environment.

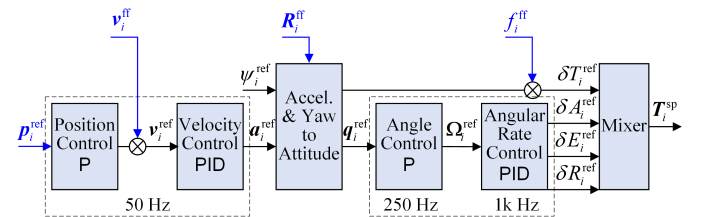


Fig. 11: Quadrotor closed-loop control architecture using the PX4 control firmware. For the  $i$ th quadrotor,  $\psi_i^{\text{ref}}$  denotes the desired yaw angle (set to zero) and  $T_i^{\text{sp}} \in \mathbb{R}^4$  denotes the thrust commands for the four motors. The superscript ff denotes 'feedforward'.

Fig. 11 illustrates the quadrotor closed-loop control architecture based on the standard PX4 control framework. The references and feedforward signals (shown in blue) for each quadrotor consist of two parts: one from the offline trajectory optimization and the other from the online feedback policies



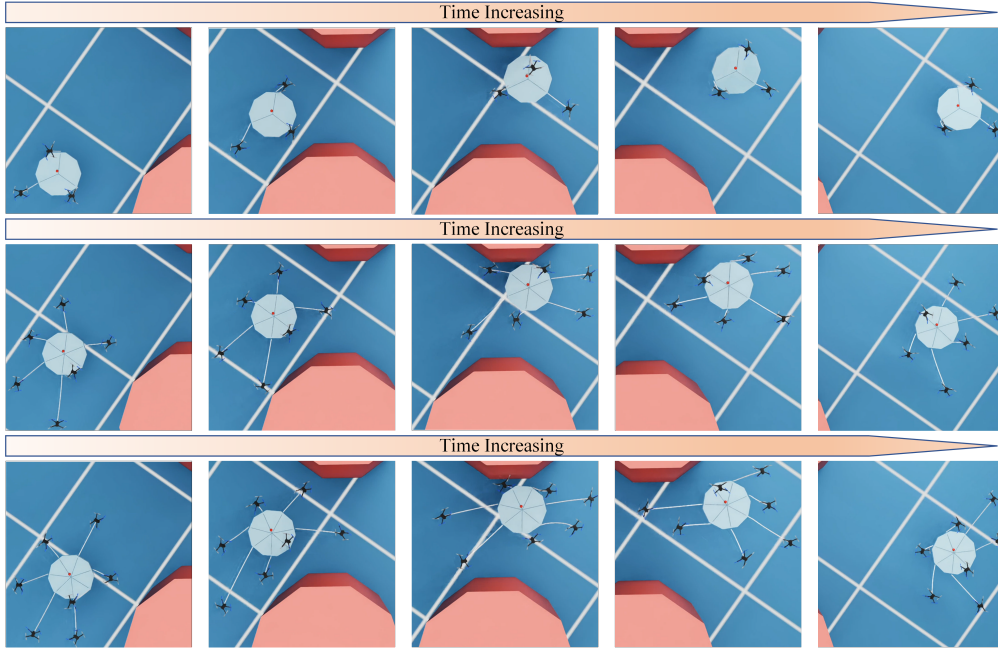


Fig. 12: Screenshots of the three multilift systems operating in the high-fidelity STIL simulation. The red point marks the load's CoM, offset from its CoG by a vector  $\mathbf{r}_g = [-30 \text{ mm}, 20 \text{ mm}]$  that is unseen in training. We set  $\alpha = 0.05$  for the three-quadrotor team and  $\alpha = 0.1$  for the other two teams. The videos are available at [https://github.com/BinghengNUS/Learning\\_to\\_Coordinate\\_1/tree/main](https://github.com/BinghengNUS/Learning_to_Coordinate_1/tree/main).

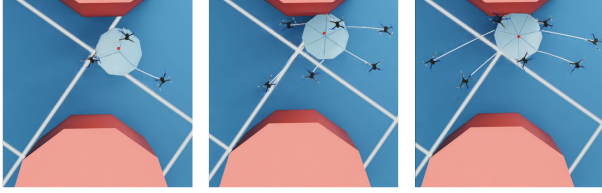


Fig. 13: Screenshots of the three teams in the high-fidelity SITL simulation when passing through the obstacles without the load closed-loop control.

provided by DDP. The latter improves the robustness of our method against model uncertainties in the load dynamics. Using the load's current state  $\mathbf{x}_{l,k}$  and the feedback gain  $\hat{\mathbf{K}}_{l,k}^*$  from its DDP subproblem, we achieve the load closed-loop control by updating the cable references as follows:

$$\delta \mathbf{t}_k = \alpha \mathbf{P}^\dagger \hat{\mathbf{K}}_{l,k}^* (\mathbf{x}_{l,k} - \mathbf{x}_{l,k}^*), \quad (63a)$$

$$\mathbf{d}_{i,k}^{\text{ref}} = \frac{t_i^* \mathbf{d}_{i,k}^* + \delta \mathbf{t}_{i,k}}{\|t_i^* \mathbf{d}_{i,k}^* + \delta \mathbf{t}_{i,k}\|}, \quad (63b)$$

where the quantities with  $*$  denote the optimal values from the offline trajectory optimization. The quadrotor's reference  $\mathbf{p}_{i,k}^{\text{ref}}$  and the feedforward signals are computed from the cable length constraint (53) and the multilift geometric controller [23], using  $\mathbf{x}_{l,k}^*$ ,  $\mathbf{d}_{i,k}^{\text{ref}}$ , and  $\mathbf{u}_{i,k}^*$ . In (63a), we scale the feedback law with a discounted factor  $\alpha \in [0, 1]$  to avoid collisions between quadrotors that could arise from aggressive  $\delta \mathbf{t}_k$ . Fig. 12 shows that a small  $\alpha \leq 0.1$  suffices for the system to track the references and adjust its formation to avoid collisions, demonstrating the dynamic feasibility of the offline trajectories and the scalability of L2C to different team sizes. When  $\alpha = 0$ , the three-quadrotor team can still pass through the obstacles without collision, but collisions occur for the other two teams (Fig. 13). This highlights the advantage of DDP

feedback policies and the system's sensitivity to the load model uncertainties from the cable-driven inter-agent constraints, both of which become more evident in large-scale multilift systems.

## VII. DISCUSSION AND CONCLUSION

This paper proposed L2C, a general framework that meta-learns key hyperparameters in ADMM-DDP-based multi-agent distributed trajectory optimization, enabling adaptation across diverse tasks and agent counts. These hyperparameters are modeled by lightweight, agent-wise neural networks and trained efficiently by differentiating end-to-end through the ADMM-DDP pipeline across multiple tasks. The key insights are twofold. First, DDP trajectory gradients correspond to the optimal solutions of a matrix-valued LQR, which can be efficiently constructed and solved by reusing DDP intermediate results such as Riccati recursions and feedback gains. Second, distributed matrix-valued LQR problems across agents can be coordinated via an auxiliary ADMM framework that enforces gradient-matching constraints, mirroring the ADMM structure in the forward pass and becoming convex under mild conditions. Through extensive high-fidelity simulations on multilift systems, we have demonstrated that L2C achieves efficient training, outperforms state-of-the-art methods in gradient computation efficiency, and meta-learns dynamically feasible trajectories that reconfigure system formations in tight spaces to avoid collisions while adapting to diverse tasks and quadrotor counts.

Future work will explore meta-learning the ADMM-DDP pipeline in a closed-loop manner to reduce the gap between trajectory optimization and downstream feedback control, as well as conducting physical experiments to further validate the effectiveness of L2C.

## APPENDIX

## A. Proof of Lemma 1

We begin by establishing the equivalence between the DBP conditions and the differential PMP conditions. Expanding the coefficient matrices on the right-hand side (R.H.S.) of (27a) (after specializing to the single-agent case) yields the following expression:

$$\begin{aligned} \frac{dV_{x,k}}{d\theta} = & \left[ \ell_{xx,k}^* + V_{x\otimes,k+1} f_{xx,k}^* + f_{x,k}^{*,\top} V_{xx,k+1} f_{x,k}^* \right] \frac{dx_k^*}{d\theta} \\ & + \left[ \ell_{xu,k}^* + V_{x\otimes,k+1} f_{xu,k}^* + f_{x,k}^{*,\top} V_{xu,k+1} f_{u,k}^* \right] \frac{du_k^*}{d\theta} \\ & + \left[ \ell_{x\theta,k}^* + V_{x\otimes,k+1} f_{x\theta,k}^* + f_{x,k}^{*,\top} V_{x\theta,k+1} f_{\theta,k}^* \right. \\ & \left. + f_{x,k}^{*,\top} V_{x\theta,k+1} \right]. \end{aligned} \quad (64)$$

By comparing the first two terms in each square bracket with the Hamiltonian  $\mathcal{H}_k$ , and using the key relation  $\lambda_k^* = V_{x,k}$ , we observe that these terms correspond exactly to the Hessians  $H_{xx,k}^*$ ,  $H_{xu,k}^*$ , and  $H_{x\theta,k}^*$  of the Hamiltonian. Consequently, (64) becomes:

$$\begin{aligned} \frac{dV_{x,k}}{d\theta} = & H_{xx,k}^* \frac{dx_k^*}{d\theta} + H_{xu,k}^* \frac{du_k^*}{d\theta} + H_{x\theta,k}^* \\ & + f_{x,k}^{*,\top} \left[ V_{xx,k+1} \frac{dx_{k+1}^*}{d\theta} + V_{x\theta,k+1} \right], \end{aligned} \quad (65)$$

after (27c) is applied. The terms within the square bracket in (65) satisfy

$$\frac{dV_{x,k+1}}{d\theta} = V_{xx,k+1} \frac{dx_{k+1}^*}{d\theta} + V_{x\theta,k+1}. \quad (66)$$

By substituting (66) and using  $\lambda_k^* = V_{x,k}$  again, the resulting (65) coincides exactly with (30a). Applying the same reasoning to (27b) yields its equivalence to (30b). This completes the proof of the equivalence. Next, we proceed to show that the matrix-valued LQR system can also be constructed based on the DBP conditions.

The Bellman optimality equation of the LQR system (31) at the optimal solutions takes the following form:

$$\begin{aligned} \bar{V}_k(\mathbf{X}_k^*) = & \text{tr} \left( \frac{1}{2} \begin{bmatrix} \mathbf{X}_k^* \\ \mathbf{U}_k^* \end{bmatrix}^\top \begin{bmatrix} H_{xx,k}^* & H_{xu,k}^* \\ H_{ux,k}^* & H_{uu,k}^* \end{bmatrix} \begin{bmatrix} \mathbf{X}_k^* \\ \mathbf{U}_k^* \end{bmatrix} \right. \\ & \left. + \begin{bmatrix} H_{x\theta,k}^* \\ H_{u\theta,k}^* \end{bmatrix}^\top \begin{bmatrix} \mathbf{X}_k^* \\ \mathbf{U}_k^* \end{bmatrix} \right) + \bar{V}_{k+1}(\mathbf{X}_{k+1}^*). \end{aligned} \quad (67)$$

Inspired by  $\bar{V}_N = \text{tr} \left( \frac{1}{2} \mathbf{X}_N^{*,\top} H_{xx,N}^* \mathbf{X}_N^* + H_{x\theta,N}^{*,\top} \mathbf{X}_N^* \right)$ , we define the value function at step  $k$  as

$$\bar{V}_k(\mathbf{X}_k^*) = \text{tr} \left( \frac{1}{2} \mathbf{X}_k^{*,\top} V_{xx,k} \mathbf{X}_k^* + V_{x\theta,k}^\top \mathbf{X}_k^* + V_{\theta\theta,k} \right), \quad (68)$$

where  $V_{\theta\theta,k}$  is the accumulated, state-independent matrix from time step  $k$  to the terminal time  $N$ , and satisfies  $V_{\theta\theta,N} = 0$ .

Differentiating both sides of (67) w.r.t.  $\mathbf{X}_k^*$  and  $\mathbf{U}_k^*$ , respectively, using matrix calculus and (68), we have the following first-order optimality conditions:

$$\begin{aligned} \frac{d\bar{V}_k}{d\mathbf{X}_k^*} = & H_{xx,k}^* \mathbf{X}_k^* + H_{xu,k}^* \mathbf{U}_k^* + H_{x\theta,k}^* \\ & + f_{x,k}^{*,\top} \left[ V_{xx,k+1} (f_{x,k}^* \mathbf{X}_k^* + f_{u,k}^* \mathbf{U}_k^* + f_{\theta,k}^*) \right. \\ & \left. + V_{x\theta,k+1} \right] \end{aligned} \quad (69a)$$

$$\begin{aligned} 0 = & H_{ux,k}^* \mathbf{X}_k^* + H_{uu,k}^* \mathbf{U}_k^* + H_{u\theta,k}^* \\ & + f_{u,k}^{*,\top} \left[ V_{xx,k+1} (f_{x,k}^* \mathbf{X}_k^* + f_{u,k}^* \mathbf{U}_k^* + f_{\theta,k}^*) \right. \\ & \left. + V_{x\theta,k+1} \right] \end{aligned} \quad (69b)$$

$$\mathbf{X}_{k+1}^* = f_{x,k}^* \mathbf{X}_k^* + f_{u,k}^* \mathbf{U}_k^* + f_{\theta,k}^*. \quad (69c)$$

Compared with (65), (69a) matches (27a). The same reasoning applies to (69b), establishing its equivalence to (27b). We thus conclude that Bellman's principle (69) coincides with the DBP conditions (27) and (32) holds. This completes the proof.

## B. Proof of Lemma 2

We prove the analytical gradients in Lemma 2 by solving the auxiliary matrix-valued LQR problem (31) using Bellman's principle. Based on the definition of the value function in (68), the cost-to-go of (31) can be expressed in the following form:

$$\begin{aligned} \bar{Q}_k = & \text{tr} \left( \frac{1}{2} \begin{bmatrix} \mathbf{X}_k \\ \mathbf{U}_k \end{bmatrix}^\top \begin{bmatrix} H_{xx,k}^* & H_{xu,k}^* \\ H_{ux,k}^* & H_{uu,k}^* \end{bmatrix} \begin{bmatrix} \mathbf{X}_k \\ \mathbf{U}_k \end{bmatrix} \right. \\ & \left. + \begin{bmatrix} H_{x\theta,k}^* \\ H_{u\theta,k}^* \end{bmatrix}^\top \begin{bmatrix} \mathbf{X}_k \\ \mathbf{U}_k \end{bmatrix} \right) \\ & + \text{tr} \left( \frac{1}{2} \mathbf{X}_{k+1}^\top V_{xx,k+1} \mathbf{X}_{k+1} \right. \\ & \left. + V_{x\theta,k+1}^\top \mathbf{X}_{k+1} + V_{\theta\theta,k+1} \right). \end{aligned} \quad (70)$$

Plugging the dynamics (69c) into (70) and setting  $\frac{\partial \bar{Q}_k}{\partial \mathbf{U}_k} = 0$  yields the matrix-valued optimal control:

$$\mathbf{U}_k^* = -Q_{uu,k}^{*,-1} Q_{ux,k}^* \mathbf{X}_k - Q_{uu,k}^{*,-1} Q_{u\theta,k}^* \quad (71)$$

where  $Q_{ux,k}^* = H_{ux,k}^* + f_{u,k}^{*,\top} V_{xx,k+1} f_{u,k}^*$ ,  $Q_{ux,k}^* = H_{ux,k}^* + f_{u,k}^{*,\top} V_{xx,k+1} f_{u,k}^*$ , and  $Q_{u\theta,k}^* = H_{u\theta,k}^* + f_{u,k}^{*,\top} V_{x\theta,k+1} + f_{u,k}^{*,\top} V_{xx,k+1} f_{\theta,k}^*$ . Plugging  $\mathbf{U}_k^*$  into (70) and comparing the resulting  $\bar{Q}_k$  with (68) yields the following two Riccati recursions:

$$V_{xx,k} = Q_{xx,k}^* - Q_{ux,k}^{*,\top} Q_{uu,k}^{*,-1} Q_{ux,k}^* \quad (72a)$$

$$V_{x\theta,k} = Q_{x\theta,k}^* - Q_{ux,k}^{*,\top} Q_{uu,k}^{*,-1} Q_{u\theta,k}^* \quad (72b)$$

where  $Q_{xx,k}^* = H_{xx,k}^* + f_{x,k}^{*,\top} V_{xx,k+1} f_{x,k}^*$ ,  $Q_{x\theta,k}^* = H_{x\theta,k}^* + f_{x,k}^{*,\top} V_{x\theta,k+1} + f_{x,k}^{*,\top} V_{xx,k+1} f_{\theta,k}^*$ ,  $V_{xx,N} = \ell_{xx,N}^*$  and  $V_{x\theta,N} = \ell_{x\theta,N}^*$  are the terminal conditions. We observe that the two recursions (72a) and (18b) are identical. This justifies the reuse of  $V_{xx,k}$ . The matrix-valued optimal control law (71) comprises a feedback gain and a feedforward gain, and shares structural similarity with the DDP control law given in (17). In

particular, the feedback gain stabilizes the gradient computation and coincides with the DDP gain  $\mathbf{K}_k = -\mathbf{Q}_{uu,k}^{*-1} \mathbf{Q}_{xu,k}^\top$ . This confirms the reuse of  $\mathbf{K}_k$ , and completes the proof.

Note that it is unnecessary to compute the Riccati recursion for  $\mathbf{V}_{\theta\theta,k}$ , as it plays no role in computing  $\mathbf{U}_k^*$ . This leads to significantly higher computational efficiency compared to the recent gradient computation method proposed in [38], which additionally requires computing the trajectory of  $\mathbf{V}_{\theta\theta,k}$ .

### C. Proof of Lemma 3

Using  $\mathcal{H}_{i,k}$ ,  $\mathcal{L}_k$ , and  $\mathcal{L}_N$ , we can rewrite the Hessian coefficient matrices in the cost functions of Auxiliary Subsystems 1 and 2 as  $\hat{H}_{\tau_i\tau_i,k}^{*,a} = H_{\tau_i\tau_i,k}^{*,a} + \rho_i \mathbf{I}_{n_i+m_i}$ ,  $\hat{L}_{\tilde{\tau}\tilde{\tau},k}^{*,a} = L_{\tilde{\tau}\tilde{\tau},k}^{*,a} + \text{Blkdiag}[\rho_i \mathbf{I}_{n_i+m_i}]_{i=1}^n$ , and  $\hat{L}_{\tilde{x}\tilde{x},N} = L_{\tilde{x}\tilde{x},N} + \text{Blkdiag}[\rho_i \mathbf{I}_{n_i}]_{i=1}^n$ , respectively. Substituting these rewritten coefficient matrices, together with (35), (42), and (43), into the cost functions, we can reformulate Auxiliary Subsystems 1 and 2 as follows:

$$\begin{aligned} \min_{\mathbf{X}_i, \mathbf{U}_i} \bar{J}_i + \sum_{k=0}^{N-1} \text{tr} \left( \frac{\rho_i}{2} \left\| \mathbf{X}_{i,k} - \tilde{\mathbf{X}}_{i,k}^{*,a} + \frac{1}{\rho_i} \frac{d\lambda_{i,k}^a}{d\theta} \right\|_2^2 \right. \\ \left. + \frac{\rho_i}{2} \left\| \mathbf{U}_{i,k} - \tilde{\mathbf{U}}_{i,k}^{*,a} + \frac{1}{\rho_i} \frac{d\xi_{i,k}^a}{d\theta} \right\|_2^2 \right) \\ + \text{tr} \left( \frac{\rho_i}{2} \left\| \mathbf{X}_{i,N} - \tilde{\mathbf{X}}_{i,N}^{*,a} + \frac{1}{\rho_i} \frac{d\lambda_{i,N}^a}{d\theta} \right\|_2^2 \right) \\ \text{s.t. } \mathbf{X}_{i,k+1} = f_{\mathbf{x},k}^* \mathbf{X}_{i,k} + f_{\mathbf{u},k}^* \mathbf{U}_{i,k} + f_{\theta,k}^* \text{ with } \mathbf{X}_{i,0} = \mathbf{0}, \end{aligned} \quad (73)$$

$$\begin{aligned} \min_{\tilde{\mathbf{X}}_k, \tilde{\mathbf{U}}_k} \bar{J}_k + \sum_{i=1}^n \text{tr} \left( \frac{\rho_i}{2} \left\| \mathbf{X}_{i,k}^{*,a+1} - \tilde{\mathbf{X}}_{i,k} + \frac{1}{\rho_i} \frac{d\lambda_{i,k}^a}{d\theta} \right\|_2^2 \right. \\ \left. + \frac{\rho_i}{2} \left\| \mathbf{U}_{i,k}^{*,a+1} - \tilde{\mathbf{U}}_{i,k} + \frac{1}{\rho_i} \frac{d\xi_{i,k}^a}{d\theta} \right\|_2^2 \right), \\ \min_{\tilde{\mathbf{X}}_N, \tilde{\mathbf{U}}_N} \bar{J}_N + \sum_{i=1}^n \text{tr} \left( \frac{\rho_i}{2} \left\| \mathbf{X}_{i,N}^{*,a+1} - \tilde{\mathbf{X}}_{i,N} + \frac{1}{\rho_i} \frac{d\lambda_{i,N}^a}{d\theta} \right\|_2^2 \right). \end{aligned} \quad (74)$$

Together with (43), these reformulated subsystems constitute exactly the aforementioned ADMM framework for Problem (44). This completes the proof.

### D. Proof of Theorem 2

#### Step 1: Control Law and Gain Perturbation

For the auxiliary matrix-valued LQR subsystem (36), the optimal gradient control laws under truncated ADMM and converged ADMM are

$$\mathbf{U}_{i,k}^{*,a_{tc}} = \hat{\mathbf{K}}_{i,k}^{a_{tc}} \mathbf{X}_{i,k}^{*,a_{tc}} + \hat{\mathbf{K}}_{i,k}^{\text{ff},a_{tc}}, \quad (75a)$$

$$\mathbf{U}_{i,k}^{*,a_{fp}} = \hat{\mathbf{K}}_{i,k}^{a_{fp}} \mathbf{X}_{i,k}^{*,a_{fp}} + \hat{\mathbf{K}}_{i,k}^{\text{ff},a_{fp}}. \quad (75b)$$

Subtracting (75b) from (75a) gives the control perturbation:

$$\Delta \mathbf{U}_{i,k} = \hat{\mathbf{K}}_{i,k}^{a_{tc}} \Delta \mathbf{X}_{i,k} + \Delta \hat{\mathbf{K}}_{i,k} \mathbf{X}_{i,k}^{*,a_{fp}} + \Delta \hat{\mathbf{K}}_{i,k}^{\text{ff}}. \quad (76)$$

where  $\Delta \hat{\mathbf{K}}_{i,k} = \hat{\mathbf{K}}_{i,k}^{a_{tc}} - \hat{\mathbf{K}}_{i,k}^{a_{fp}}$  and similarly for  $\Delta \hat{\mathbf{K}}_{i,k}^{\text{ff}}$ . While most classical sensitivity analyses of Riccati equations address

the infinite-horizon algebraic setting [70], [71], the control gains in the finite-horizon recursive case are also Lipschitz bounded. This is because the backward Riccati recursions, such as (72a) and (72b), involve differentiable matrix operations. Specifically, there exist constants  $C_{i,k}$ ,  $C_{i,k}^{\text{ff}} > 0$  such that

$$\|\Delta \hat{\mathbf{K}}_{i,k}\| \leq C_{i,k} \|\delta \tau_{i,k}\|, \quad \|\Delta \hat{\mathbf{K}}_{i,k}^{\text{ff}}\| \leq C_{i,k}^{\text{ff}} \|\delta \tau_{i,k}\|. \quad (77)$$

Thus, the norm of (76) is upper-bounded by:

$$\|\Delta \mathbf{U}_{i,k}\| \leq \|\hat{\mathbf{K}}_{i,k}^{a_{tc}}\| \|\Delta \mathbf{X}_{i,k}\| + C_{i,k}' \|\delta \tau_{i,k}\|, \quad (78)$$

where  $C_{i,k}' = C_{i,k} \|\mathbf{X}_{i,k}^{*,a_{fp}}\| + C_{i,k}^{\text{ff}}$ .

#### Step 2: Dynamics Perturbation

Applying the same perturbation analysis to the dynamics in (36) as was done for the control laws, and substituting (76) into the resulting expression, we obtain:

$$\Delta \mathbf{X}_{i,k+1} = \mathbf{A}_{i,k} \Delta \mathbf{X}_{i,k} + \Phi_{i,k}. \quad (79)$$

where

$$\mathbf{A}_{i,k} = f_{\mathbf{x},k}^{*,a_{tc}} + f_{\mathbf{u},k}^{*,a_{tc}} \hat{\mathbf{K}}_{i,k}^{a_{tc}}, \quad (80a)$$

$$\begin{aligned} \Phi_{i,k} = f_{\mathbf{u},k}^{*,a_{tc}} \Delta \hat{\mathbf{K}}_{i,k} \mathbf{X}_{i,k}^{*,a_{fp}} + f_{\mathbf{u},k}^{*,a_{tc}} \Delta \hat{\mathbf{K}}_{i,k}^{\text{ff}} \\ + \Delta f_{\mathbf{x},k}^* \mathbf{X}_{i,k}^{*,a_{fp}} + \Delta f_{\mathbf{u},k}^* \mathbf{U}_{i,k}^{*,a_{fp}} + \Delta f_{\theta,k}^*. \end{aligned} \quad (80b)$$

Before propagating this recursion, we need to bound the bias term  $\Phi_{i,k}$  stage-wise to control the corresponding accumulated error. Applying the submultiplicativity of the operator norm, the gain-perturbation bounds (77), and the assumed Lipschitz-type bounds (48) to  $\Phi_{i,k}$ , we have

$$\begin{aligned} \|f_{\mathbf{u},k}^{*,a_{tc}} \Delta \hat{\mathbf{K}}_{i,k} \mathbf{X}_{i,k}^{*,a_{fp}}\| &\leq \|f_{\mathbf{u},k}^{*,a_{tc}}\| C_{i,k} \|\mathbf{X}_{i,k}^{*,a_{fp}}\| \|\delta \tau_{i,k}\|, \\ \|f_{\mathbf{u},k}^{*,a_{tc}} \Delta \hat{\mathbf{K}}_{i,k}^{\text{ff}}\| &\leq \|f_{\mathbf{u},k}^{*,a_{tc}}\| C_{i,k}^{\text{ff}} \|\delta \tau_{i,k}\|, \\ \|\Delta f_{\mathbf{x},k}^* \mathbf{X}_{i,k}^{*,a_{fp}}\| &\leq L_6 \|\mathbf{X}_{i,k}^{*,a_{fp}}\| \|\delta \tau_{i,k}\|, \\ \|\Delta f_{\mathbf{u},k}^* \mathbf{U}_{i,k}^{*,a_{fp}}\| &\leq L_7 \|\mathbf{U}_{i,k}^{*,a_{fp}}\| \|\delta \tau_{i,k}\|, \\ \|\Delta f_{\theta,k}^*\| &\leq L_8 \|\delta \tau_{i,k}\|. \end{aligned} \quad (81)$$

Define

$$X_{\max} := \max_{0 \leq k \leq N} \|\mathbf{X}_{i,k}^{*,a_{fp}}\|, \quad U_{\max} := \max_{0 \leq k \leq N-1} \|\mathbf{U}_{i,k}^{*,a_{fp}}\|.$$

By collecting terms, we have

$$\|\Phi_{i,k}\| \leq \beta_{i,k} \|\delta \tau_{i,k}\|, \quad (82)$$

where

$$\beta_{i,k} := \|f_{\mathbf{u},k}^{*,a_{tc}}\| (C_{i,k} X_{\max} + C_{i,k}^{\text{ff}}) + L_6 X_{\max} + L_7 U_{\max} + L_8.$$

#### Step 3: Error Propagation for $\Delta \mathbf{X}_{i,k}$

Define  $\alpha_{i,k} := \|\mathbf{A}_{i,k}\|$  (finite for each  $k$ ). With  $\Delta \mathbf{X}_{i,0} = \mathbf{0}$  (as  $\mathbf{X}_{i,0}^*$  is independent of  $\theta$ ), iterating the recursion yields

$$\Delta \mathbf{X}_{i,k} = \sum_{t=0}^{k-1} \left( \prod_{s=t+1}^{k-1} \mathbf{A}_{i,s} \right) \Phi_{i,t}. \quad (83)$$

Taking norms and using the bound on  $\Phi_{i,t}$  yields

$$\|\Delta \mathbf{X}_{i,k}\| \leq \sum_{t=0}^{k-1} \underbrace{\left( \prod_{s=t+1}^{k-1} \alpha_{i,s} \right) \beta_{i,t}}_{:= \sum_{t=0}^{k-1} \Lambda_i(k,t)} \|\delta \tau_{i,t}\| \quad (84)$$



Define  $L_{X,i,k} := \max_{0 \leq t < k} \Lambda_i(k, t)$ , so

$$\|\Delta \mathbf{X}_{i,k}\| \leq L_{X,i,k} \sum_{t=0}^{k-1} \|\delta \boldsymbol{\tau}_{i,t}\|. \quad (85)$$

*Step 4: Error Propagation for  $\Delta \mathbf{U}_{i,k}$*

Substituting the state bound (84) into (78) yields

$$\begin{aligned} \|\Delta \mathbf{U}_{i,k}\| &\leq \|\hat{\mathbf{K}}_{i,k}^{a_{tc}}\| \sum_{t=0}^{k-1} \Lambda_i(k, t) \|\delta \boldsymbol{\tau}_{i,t}\| + C'_{i,k} \|\delta \boldsymbol{\tau}_{i,k}\| \\ &:= \sum_{t=0}^k M_i(k, t) \|\delta \boldsymbol{\tau}_{i,t}\|, \end{aligned} \quad (86)$$

where  $M_i(k, t) := \|\hat{\mathbf{K}}_{i,k}^{a_{tc}}\| \Lambda_i(k, t)$  for  $t < k$  and  $M_i(k, k) := C'_{i,k}$ . Define  $L_{U,i,k} := \max_{0 \leq t \leq k} M_i(k, t)$ . Then

$$\|\Delta \mathbf{U}_{i,k}\| \leq L_{U,i,k} \sum_{t=0}^k \|\delta \boldsymbol{\tau}_{i,t}\|. \quad (87)$$

This completes the proof.

## REFERENCES

- [1] G. Li, X. Liu, and G. Loianno, "Rotortm: A flexible simulator for aerial transportation and manipulation," *IEEE Transactions on Robotics*, vol. 40, pp. 831–850, 2024.
- [2] A. Yamashita, T. Arai, J. Ota, and H. Asama, "Motion planning of multiple mobile robots for cooperative manipulation and transportation," *IEEE Transactions on Robotics and Automation*, vol. 19, no. 2, pp. 223–237, 2003.
- [3] J. Kim, J. Lee, and A. D. Ames, "Safety-critical coordination for cooperative legged locomotion via control barrier functions," in *2023 IEEE/RSJ International Conference on Intelligent Robots and Systems (IROS)*, 2023, pp. 2368–2375.
- [4] Q. Li and S. Payandeh, "Centralized cooperative planning for dynamic multi-agent planar manipulation," in *Proceedings of the 41st IEEE Conference on Decision and Control*, 2002., vol. 3, 2002, pp. 2836–2841 vol.3.
- [5] S. Boyd, N. Parikh, E. Chu, B. Peleato, J. Eckstein *et al.*, "Distributed optimization and statistical learning via the alternating direction method of multipliers," *Foundations and Trends® in Machine Learning*, vol. 3, no. 1, pp. 1–122, 2011.
- [6] S. Choudhary, L. Carlone, H. I. Christensen, and F. Dellaert, "Exactly sparse memory efficient slam using the multi-block alternating direction method of multipliers," in *2015 IEEE/RSJ International Conference on Intelligent Robots and Systems (IROS)*, 2015, pp. 1349–1356.
- [7] R. Ni, Z. Pan, and X. Gao, "Robust multi-robot trajectory optimization using alternating direction method of multiplier," *IEEE Robotics and Automation Letters*, vol. 7, no. 3, pp. 5950–5957, 2022.
- [8] W. Tang and P. Daoutidis, "Distributed nonlinear model predictive control through accelerated parallel admm," in *2019 American Control Conference (ACC)*, 2019, pp. 1406–1411.
- [9] D. Krishnamoorthy and V. Kungurtsev, "A sensitivity assisted alternating directions method of multipliers for distributed optimization," in *2022 IEEE 61st Conference on Decision and Control (CDC)*, 2022, pp. 295–300.
- [10] A. D. Saravanos, Y. Aoyama, H. Zhu, and E. A. Theodorou, "Distributed differential dynamic programming architectures for large-scale multiagent control," *IEEE Transactions on Robotics*, vol. 39, no. 6, pp. 4387–4407, 2023.
- [11] D. M. and, "A second-order gradient method for determining optimal trajectories of non-linear discrete-time systems," *International Journal of Control*, vol. 3, no. 1, pp. 85–95, 1966.
- [12] L.-Z. Liao and C. A. Shoemaker, "Convergence in unconstrained discrete-time differential dynamic programming," *IEEE Transactions on Automatic Control*, vol. 36, no. 6, pp. 692–706, 1991.
- [13] —, "Advantages of differential dynamic programming over newton's method for discrete-time optimal control problems," Cornell University, Tech. Rep., 1992.
- [14] I.-W. Park, Y.-D. Hong, B.-J. Lee, and J.-H. Kim, "Generating optimal trajectory of humanoid arm that minimizes torque variation using differential dynamic programming," in *2012 IEEE International Conference on Robotics and Automation*, 2012, pp. 1316–1321.
- [15] Y. Aoyama, G. Boutselis, A. Patel, and E. A. Theodorou, "Constrained differential dynamic programming revisited," in *2021 IEEE International Conference on Robotics and Automation (ICRA)*, 2021, pp. 9738–9744.
- [16] W. Jallet, A. Bambade, N. Mansard, and J. Carpentier, "Constrained differential dynamic programming: A primal-dual augmented lagrangian approach," in *2022 IEEE/RSJ International Conference on Intelligent Robots and Systems (IROS)*, 2022, pp. 13 371–13 378.
- [17] G. Kim, D. Kang, J.-H. Kim, and H.-W. Park, "Contact-implicit differential dynamic programming for model predictive control with relaxed complementarity constraints," in *2022 IEEE/RSJ International Conference on Intelligent Robots and Systems (IROS)*, 2022, pp. 11 978–11 985.
- [18] S.-S. Park, Y. Min, J.-S. Ha, D.-H. Cho, and H.-L. Choi, "A distributed admm approach to non-myopic path planning for multi-target tracking," *IEEE Access*, vol. 7, pp. 163 589–163 603, 2019.
- [19] X. Zhang, Z. Cheng, J. Ma, S. Huang, F. L. Lewis, and T. H. Lee, "Semi-definite relaxation-based admm for cooperative planning and control of connected autonomous vehicles," *IEEE Transactions on Intelligent Transportation Systems*, vol. 23, no. 7, pp. 9240–9251, 2022.
- [20] N. Michael, J. Fink, and V. Kumar, "Cooperative manipulation and transportation with aerial robots," *Autonomous Robots*, vol. 30, pp. 73–86, 2011.
- [21] K. Sreenath and V. Kumar, "Dynamics, control and planning for cooperative manipulation of payloads suspended by cables from multiple quadrotor robots," *m*, vol. 1, no. r2, p. r3, 2013.
- [22] C. Masone, H. H. Bühlhoff, and P. Stegagno, "Cooperative transportation of a payload using quadrotors: A reconfigurable cable-driven parallel robot," in *2016 IEEE/RSJ International Conference on Intelligent Robots and Systems (IROS)*, 2016, pp. 1623–1630.
- [23] T. Lee, "Geometric control of quadrotor uavs transporting a cable-suspended rigid body," *IEEE Transactions on Control Systems Technology*, vol. 26, no. 1, pp. 255–264, 2018.
- [24] K. Klausen, C. Meissen, T. I. Fossen, M. Arcak, and T. A. Johansen, "Cooperative control for multirotors transporting an unknown suspended load under environmental disturbances," *IEEE Transactions on Control Systems Technology*, vol. 28, no. 2, pp. 653–660, 2020.
- [25] J. Geng and J. W. Langelaan, "Cooperative transport of a slung load using load-leading control," *Journal of Guidance, Control, and Dynamics*, vol. 43, no. 7, pp. 1313–1331, 2020.
- [26] Y. Wang, G. Yu, W. Xie, W. Zhang, and C. Silvestre, "Robust cooperative transportation of a cable-suspended payload by multiple quadrotors featuring cable-reconfiguration capabilities," *IEEE Transactions on Intelligent Transportation Systems*, vol. 25, no. 9, pp. 11 833–11 843, 2024.
- [27] B. Wang, R. Huang, and L. Zhao, "Auto-multilift: Distributed learning and control for cooperative load transportation with quadrotors," *arXiv preprint arXiv:2406.04858*, 2024.
- [28] M. Okada, L. Rigazio, and T. Aoshima, "Path integral networks: End-to-end differentiable optimal control," *arXiv preprint arXiv:1706.09597*, 2017.
- [29] B. Landry, Z. Manchester, and M. Pavone, "A differentiable augmented lagrangian method for bilevel nonlinear optimization," in *2019 Robotics: Science and Systems*, 2019, pp. 1–9.
- [30] A. Paszke, S. Gross, S. Chintala, G. Chanan, E. Yang, Z. DeVito, Z. Lin, A. Desmaison, L. Antiga, and A. Lerer, "Automatic differentiation in pytorch," in *Proceedings of the 31st Conference on Neural Information Processing Systems*. Long Beach, CA, USA: Curran Associates Inc., 2017, pp. 1–4.
- [31] B. Amos, I. D. J. Rodriguez, J. Sacks, B. Boots, and J. Z. Kolter, "Differentiable mpc for end-to-end planning and control," in *Proceedings of the 32nd International Conference on Neural Information Processing Systems*, ser. NIPS'18. Red Hook, NY, USA: Curran Associates Inc., 2018, p. 8299–8310.
- [32] T. Dinev, C. Mastalli, V. Ivan, S. Tonneau, and S. Vijayakumar, "Differentiable optimal control via differential dynamic programming," *arXiv preprint arXiv:2209.01117*, 2022.
- [33] O. Alex, A. Hassan, and A. T. Evangelos, "Differentiable robust model predictive control," in *2024 Robotics: Science and Systems*, 2024, pp. 1–22.
- [34] R. Angel, A. Elie, S. Yunlong, and S. Davide, "Actor-critic model predictive control: Differentiable optimization meets reinforcement learning," *arXiv preprint arXiv:2306.09852*, 2025.
- [35] W. Jin, Z. Wang, Z. Yang, and S. Mou, "Pontryagin differentiable programming: An end-to-end learning and control framework," in

- Advances in Neural Information Processing Systems*, H. Larochelle, M. Ranzato, R. Hadsell, M. Balcan, and H. Lin, Eds., vol. 33. Curran Associates, Inc., 2020, pp. 7979–7992.
- [36] W. Jin, S. Mou, and G. J. Pappas, “Safe pontryagin differentiable programming,” in *Advances in Neural Information Processing Systems*, M. Ranzato, A. Beygelzimer, Y. Dauphin, P. Liang, and J. W. Vaughan, Eds., vol. 34. Curran Associates, Inc., 2021, pp. 16034–16050.
- [37] Z. Liang, T. Zhou, Z. Lu, and S. Mou, “Online control-informed learning,” 2025. [Online]. Available: <https://arxiv.org/abs/2410.03924>
- [38] K. Cao, X. Xu, W. Jin, K. H. Johansson, and L. Xie, “A differential dynamic programming framework for inverse reinforcement learning,” 2024. [Online]. Available: <https://arxiv.org/abs/2407.19902>
- [39] X. Xie, J. Wu, G. Liu, Z. Zhong, and Z. Lin, “Differentiable linearized ADMM,” in *Proceedings of the 36th International Conference on Machine Learning*, ser. Proceedings of Machine Learning Research, K. Chaudhuri and R. Salakhutdinov, Eds., vol. 97. PMLR, 09–15 Jun 2019, pp. 6902–6911.
- [40] H. Sun, Y. Shi, J. Wang, H. D. Tuan, H. V. Poor, and D. Tao, “Alternating differentiation for optimization layers,” 2023.
- [41] B. Andrew and K. Roy H., “Efficient differentiable quadratic programming layers: an admm approach,” *Computational Optimization and Applications*, vol. 84, pp. 3368–3374, 2023.
- [42] H. Hu, L. Zhang, Y. Hua, C. Zhao, W. Pan, and H. Chen, “Automated hyperparameter tuning for data-driven mpc: A differentiable admm approach for enhancing vehicle stability,” *IEEE Transactions on Industrial Electronics*, pp. 1–11, 2025.
- [43] L. Zhang, Y. Sun, A. Barth, and O. Ma, “Decentralized control of multi-robot system in cooperative object transportation using deep reinforcement learning,” *IEEE Access*, vol. 8, pp. 184 109–184 119, 2020.
- [44] Z. Xia, J. Du, J. Wang, C. Jiang, Y. Ren, G. Li, and Z. Han, “Multi-agent reinforcement learning aided intelligent uav swarm for target tracking,” *IEEE Transactions on Vehicular Technology*, vol. 71, no. 1, pp. 931–945, 2022.
- [45] S. Gu, J. Grudzien Kuba, Y. Chen, Y. Du, L. Yang, A. Knoll, and Y. Yang, “Safe multi-agent reinforcement learning for multi-robot control,” *Artificial Intelligence*, vol. 319, p. 103905, 2023. [Online]. Available: <https://www.sciencedirect.com/science/article/pii/S0004370223000516>
- [46] J. Orr and A. Dutta, “Multi-agent deep reinforcement learning for multi-robot applications: A survey,” *Sensors*, vol. 23, no. 7, 2023. [Online]. Available: <https://www.mdpi.com/1424-8220/23/7/3625>
- [47] J. Zeng, A. M. Gimenez, E. Vinitsky, J. Alonso-Mora, and S. Sun, “Decentralized aerial manipulation of a cable-suspended load using multi-agent reinforcement learning,” *arXiv preprint arXiv:2508.01522*, 2025.
- [48] C. Song, S. Yoon, and V. Pavlovic, “Fast admm algorithm for distributed optimization with adaptive penalty,” in *Proceedings of the Thirtieth AAAI Conference on Artificial Intelligence*, ser. AAAI’16. AAAI Press, 2016, p. 753–759.
- [49] Y. Xu, M. Liu, Q. Lin, and T. Yang, “Admm without a fixed penalty parameter: Faster convergence with new adaptive penalization,” in *Advances in Neural Information Processing Systems*, I. Guyon, U. V. Luxburg, S. Bengio, H. Wallach, R. Fergus, S. Vishwanathan, and R. Garnett, Eds., vol. 30. Curran Associates, Inc., 2017.
- [50] M. T. MCCANN and B. Wohlberg, “Robust and simple admm penalty parameter selection,” *IEEE Open Journal of Signal Processing*, vol. 5, pp. 402–420, 2024.
- [51] J. Fink, N. Michael, S. Kim, and V. Kumar, “Planning and control for cooperative manipulation and transportation with aerial robots,” *The International Journal of Robotics Research*, vol. 30, no. 3, pp. 324–334, 2011. [Online]. Available: <https://doi.org/10.1177/0278364910382803>
- [52] J. Geng, P. Singla, and J. W. Langelaan, “Load-distribution-based trajectory planning and control for a multilift system,” *Journal of Aerospace Information Systems*, vol. 19, no. 5, pp. 366–381, 2022.
- [53] S. Sun and A. Franchi, “Nonlinear mpc for full-pose manipulation of a cable-suspended load using multiple uavs,” in *2023 International Conference on Unmanned Aircraft Systems (ICUAS)*. IEEE, 2023, pp. 969–975.
- [54] K. Wabba, J. Ortiz-Haro, M. Toussaint, and W. Hönig, “Kinodynamic motion planning for a team of multirotors transporting a cable-suspended payload in cluttered environments,” in *2024 IEEE/RSJ International Conference on Intelligent Robots and Systems (IROS)*. IEEE, 2024, pp. 12 750–12 757.
- [55] Y. Wang, J. Wang, X. Zhou, T. Yang, C. Xu, and F. Gao, “Safe and agile transportation of cable-suspended payload via multiple aerial robots,” *arXiv preprint arXiv:2501.15272*, 2025.
- [56] S. Sun, X. Wang, D. Sanalidro, A. Franchi, M. Tognon, and J. Alonso-Mora, “Agile and cooperative aerial manipulation of a cable-suspended load,” *arXiv preprint arXiv:2501.18802*, 2025.
- [57] Y. Chai, Z. Zhang, H. Yu, J. Han, Y. Fang, and X. Liang, “A trajectory planning scheme for collaborative aerial transportation systems by graph-based searching and cable tension optimization,” *IEEE/ASME Transactions on Mechatronics*, pp. 1–12, 2025.
- [58] J. Wehbeh, S. Rahman, and I. Sharf, “Distributed model predictive control for uavs collaborative payload transport,” in *2020 IEEE/RSJ International Conference on Intelligent Robots and Systems (IROS)*, 2020, pp. 11 666–11 672.
- [59] B. E. Jackson, T. A. Howell, K. Shah, M. Schwager, and Z. Manchester, “Scalable cooperative transport of cable-suspended loads with uavs using distributed trajectory optimization,” *IEEE Robotics and Automation Letters*, vol. 5, no. 2, pp. 3368–3374, 2020.
- [60] NVIDIA, “Nvidia isaac sim,” <https://developer.nvidia.com/isaac-sim>, 2022, accessed: 29-Jan-2023.
- [61] R. Bellman, “Dynamic programming,” *science*, vol. 153, no. 3731, pp. 34–37, 1966.
- [62] J. Ma, Z. Cheng, X. Zhang, Z. Lin, F. L. Lewis, and T. H. Lee, “Local learning enabled iterative linear quadratic regulator for constrained trajectory planning,” *IEEE Transactions on Neural Networks and Learning Systems*, vol. 34, no. 9, pp. 5354–5365, 2023.
- [63] A. Wächter, *An interior point algorithm for large-scale nonlinear optimization with applications in process engineering*. Carnegie Mellon University, 2002.
- [64] A. L. Dontchev and R. T. Rockafellar, *Implicit functions and solution mappings*. Springer, 2009, vol. 543.
- [65] Z. Huang, R. Hu, Y. Guo, E. Chan-Tin, and Y. Gong, “Dp-admm: Admm-based distributed learning with differential privacy,” *IEEE Transactions on Information Forensics and Security*, vol. 15, pp. 1002–1012, 2020.
- [66] S. Yeo, G. Yang, and W. Lim, “Design and analysis of cable-driven manipulators with variable stiffness,” *Mechanism and Machine Theory*, vol. 69, pp. 230–244, 2013.
- [67] J. A. Andersson, J. Gillis, G. Horn, J. B. Rawlings, and M. Diehl, “Casadi: a software framework for nonlinear optimization and optimal control,” *Mathematical Programming Computation*, vol. 11, no. 1, pp. 1–36, 2019.
- [68] D. Kingma and J. Ba, “Adam: A method for stochastic optimization,” in *in: Proceedings of the 3rd international conference for learning representations (ICLR’15)*, vol. 500, 2015.
- [69] D. Mellinger and V. Kumar, “Minimum snap trajectory generation and control for quadrotors,” in *2011 IEEE International Conference on Robotics and Automation*. IEEE, 2011, pp. 2520–2525.
- [70] J.-g. Sun, “Sensitivity analysis of the discrete-time algebraic riccati equation,” *Linear algebra and its applications*, vol. 275, pp. 595–615, 1998.
- [71] J.-G. Sun, “Perturbation theory for algebraic riccati equations,” *SIAM Journal on Matrix Analysis and Applications*, vol. 19, no. 1, pp. 39–65, 1998.